



**Borthwick, Jennifer A. and Ancellin, Nicolas and Bertrand, Sophie M. and Bingham, Ryan P. and Carter, Paul S. and Chung, Chun-wa and Churcher, Ian and Dodic, Nerina and Fournier, Charlène and Francis, Peter L. and Hobbs, Andrew and Jamieson, Craig and Pickett, Stephen D. and Smith, Sarah E. and Somers, Donald O'N. and Spitzfaden, Claus and Suckling, Colin J. and Young, Robert J. (2016) Structurally diverse mitochondrial branched chain aminotransferase (BCATm) leads with varying binding modes identified by fragment screening. *Journal of Medicinal Chemistry*, 59 (6). pp. 2452-2467. ISSN 0022-2623 , <http://dx.doi.org/10.1021/acs.jmedchem.5b01607>**

This version is available at <http://strathprints.strath.ac.uk/55944/>

**Strathprints** is designed to allow users to access the research output of the University of Strathclyde. Unless otherwise explicitly stated on the manuscript, Copyright © and Moral Rights for the papers on this site are retained by the individual authors and/or other copyright owners. Please check the manuscript for details of any other licences that may have been applied. You may not engage in further distribution of the material for any profitmaking activities or any commercial gain. You may freely distribute both the url (<http://strathprints.strath.ac.uk/>) and the content of this paper for research or private study, educational, or not-for-profit purposes without prior permission or charge.

Any correspondence concerning this service should be sent to the Strathprints administrator: [strathprints@strath.ac.uk](mailto:strathprints@strath.ac.uk)

1  
2  
3  
4  
5  
6  
7 **Structurally Diverse Mitochondrial Branched Chain Aminotransferase**  
8  
9 **(BCATm) Leads With Varying Binding Modes Identified by Fragment**  
10  
11 **Screening**  
12  
13  
14  
15

16 Jennifer A Borthwick<sup>\*1,3</sup>, Nicolas Ancellin<sup>2</sup>, Sophie M Bertrand<sup>1,3</sup>, Ryan P Bingham<sup>1</sup>, Paul S  
17 Carter<sup>1</sup>, Chun-wa Chung<sup>1</sup>, Ian Churcher<sup>1</sup>, Nerina Dodic<sup>2</sup>, Charlène Fournier<sup>1</sup>, Peter L Francis<sup>1</sup>,  
18 Andrew Hobbs<sup>1</sup>, Craig Jamieson<sup>3</sup>, Stephen D Pickett<sup>1</sup>, Sarah E Smith<sup>1</sup>, Donald O’N Somers<sup>1</sup>,  
19 Claus Spitzfaden<sup>1</sup>, Colin J Suckling<sup>3</sup>, Robert J Young<sup>1</sup>.  
20  
21  
22  
23  
24  
25

26 <sup>1</sup>*GlaxoSmithKline R&D, Medicines Research Centre, Gunnels Wood Road, Stevenage,*  
27 *Hertfordshire, SG1 2NY, UK.*  
28  
29  
30  
31

32 <sup>2</sup>*GlaxoSmithKline R&D, Les Ulis, Centre de Recherche, 25,27 Avenue du Québec, 91140*  
33 *Villebon sur Yvette, France.*  
34  
35  
36

37 <sup>3</sup>*Department of Pure and Applied Chemistry, University of Strathclyde, 295 Cathedral Street,*  
38 *Glasgow, G1 1XL.*  
39  
40  
41  
42  
43

44 **Abstract**  
45  
46  
47

48 Inhibitors of mitochondrial branched chain aminotransferase (BCATm), identified using  
49 fragment screening, are described. This was carried out using a combination of STD-NMR,  
50 thermal melt ( $T_m$ ) and biochemical assays to identify compounds that bound to BCATm, which  
51 were subsequently progressed to X-ray crystallography, where a number of exemplars showed  
52 significant diversity in their binding modes. The hits identified were supplemented by searching  
53  
54  
55  
56  
57  
58  
59  
60

1  
2  
3 and screening of additional analogues, which enabled the gathering of further X-ray data where  
4  
5 the original hits had not produced liganded structures. The fragment hits were optimised using  
6  
7 structure-based design, with some transfer of information between series, which enabled the  
8  
9 identification of ligand efficient lead molecules with micromolar levels of inhibition, cellular  
10  
11 activity, and good solubility.  
12  
13

## 14 15 16 17 **Introduction**

18  
19  
20 Mitochondrial branched chain aminotransferase (BCATm) is a metabolic enzyme which  
21  
22 converts the branched chain amino acids (BCAAs), leucine, isoleucine and valine into their  
23  
24 corresponding  $\alpha$ -keto acids. Over the past few years, evidence has appeared linking this enzyme  
25  
26 to obesity in animals and humans; accordingly inhibition of this enzyme has potential as a  
27  
28 treatment for obesity and related diseases. The BCATm isoform is expressed ubiquitously, with  
29  
30 very high levels in the stomach, pancreas and salivary glands, consistent with its role in protein  
31  
32 metabolism.<sup>1</sup> Interestingly, BCATm knock-out mice are resistant to high-fat diet induced obesity  
33  
34 and diabetes;<sup>2</sup> these effects are believed to be caused by the establishment of an energy  
35  
36 consuming cycle of protein synthesis and degradation. This phenotype is similar to that observed  
37  
38 in humans who consume high protein diets or BCAA supplements and experience increased  
39  
40 energy expenditure, lower appetite and ultimately, lower body weights.<sup>2</sup> The role of BCATm and  
41  
42 BCAAs in the aetiology of obesity is complex and not fully understood; knock-out and dietary  
43  
44 studies discussed above, where high levels of BCAA appear to be associated with reduced risk of  
45  
46 becoming obese, are complicated by studies of obese animals. Genetically mutated obese rodents  
47  
48 and diet-induced obese mice and humans have all been shown to have reduced BCATm  
49  
50 expression, resulting in higher BCAA levels than lean animals.<sup>3</sup>  
51  
52  
53  
54  
55  
56  
57  
58  
59  
60

1  
2  
3 The search for inhibitors of BCATm at GSK was pursued using three complementary methods;  
4 fragment screening, high throughput screening (HTS) and encoded library technology. This  
5 paper describes the diversity of chemical matter, displaying distinct binding modes discovered  
6 by fragment screening. Hybridization of one of these hits with an HTS hit led to a potent *in vivo*  
7 active series<sup>4</sup> and a further series was identified by encoded library technology.<sup>5</sup> Together, this  
8 package of work has shed much light on the variable binding modes observed with BCATm and  
9 is beginning to shed some light on the effects of specific pharmacological inhibition of BCATm  
10 by small molecules and the role of this enzyme in disease.  
11  
12  
13  
14  
15  
16  
17  
18  
19  
20  
21  
22

23 In a commentary<sup>6</sup> on our Fragment Assisted Drug Design<sup>7</sup> paper, the difficulty of the target  
24 was highlighted, as was the importance of having diverse chemical matter with appropriate *in*  
25 *vivo* activities to interrogate a target; this paper illustrates structural information describing  
26 diverse binding modes observed. In fragment screening, the lack of overlap between screening  
27 methods has been acknowledged<sup>8</sup>; this was observed in the progression of hits identified by the  
28 various methods in this fragment screen, perhaps compounded by the diversity of binding modes.  
29  
30  
31  
32  
33  
34  
35  
36  
37

38 The fragment hits were clustered according to their distinct binding modes. Importantly, this  
39 study provides new structural understanding of this enzyme, with several binding pockets  
40 identified by the fragment screen, which were not occupied by either of the other series<sup>4,5</sup>.  
41 Additionally, further optimisation efforts on two of the fragment hit series are described, which  
42 represent useful starting points and give important structural pointers to enable the identification  
43 of structurally novel tools for further pharmacological studies.  
44  
45  
46  
47  
48  
49  
50  
51  
52

## 53 **Results and Discussion**

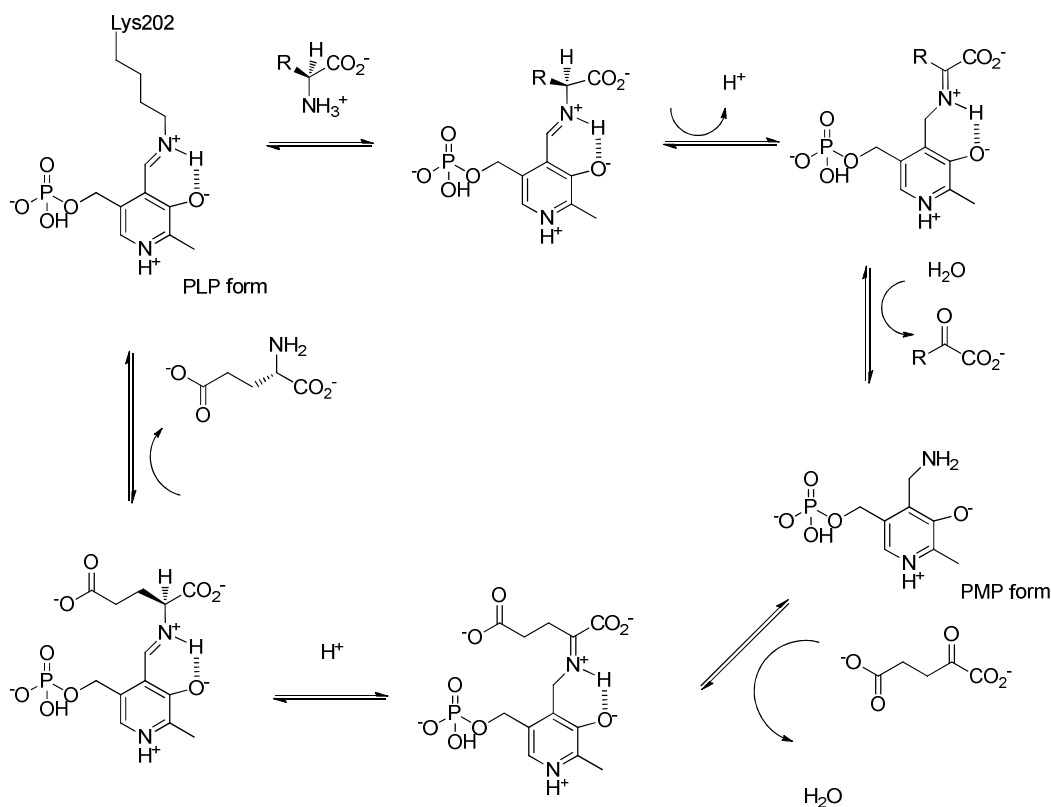
### 54 **Fragment Screening**

1  
2  
3  
4  
5  
6  
7  
8  
9  
10  
11  
12  
13  
14  
15  
16  
17  
18  
19  
20  
21  
22  
23  
24  
25  
26  
27  
28  
29  
30  
31  
32  
33  
34  
35  
36  
37  
38  
39  
40  
41  
42  
43  
44  
45  
46  
47  
48  
49  
50  
51  
52  
53  
54  
55  
56  
57  
58  
59  
60

FBDD techniques have become an integral part of the drug discovery process during the last decade.<sup>7,9,10</sup> Standard components of the FBDD methodology include the use of biophysical screening and X-ray crystallography to enable the identification, optimisation and designed growth of inherently weakly binding ligands into potent lead molecules.<sup>11</sup> Commonly, these methods have used a single form of the protein, for example, the apo or a cofactor bound state.

However, during enzyme turnover in solution, the dynamic changes in protein conformation and biochemical state present a number of potential binding opportunities. The use of a single form for screening in a binding assay may restrict the type of compounds that can be detected and characterised. In the extreme case, this arbitrary choice may preclude sampling the most tractable form of the enzyme. During the catalytic cycle (Scheme 1) PLP and PMP cofactor bound forms of BCATm are sampled. Pragmatically we therefore used both PLP and PMP forms in our studies where possible, as these can both be stably isolated.

At the start of the cycle, the cofactor pyridoxal phosphate (PLP) is covalently bound to the enzyme *via* a lysine residue (Lys-202) (Scheme 1).<sup>12</sup> This lysine is then displaced by the  $\alpha$ -amine of an incoming BCAA substrate. The imine formed is hydrolysed to the corresponding  $\alpha$ -keto acid. In the course of the reaction, the co-factor is released from its covalent bond to the enzyme as pyridoxamine phosphate (PMP). A complementary half-reaction occurs to complete the cycle, whereby  $\alpha$ -ketoglutarate is transaminated to glutamate and the PLP form of the enzyme is regenerated. It was possible to characterise both the PLP and PMP forms of the enzyme (e.g. spectroscopically or by mass spectrometry) and to interconvert between these using an excess of either leucine or  $\alpha$ -keto glutarate as appropriate.



**Scheme 1: Reaction cycle catalysed by BCATm**

A functional biochemical assay was designed to detect inhibitors of this pathway, making use of a coupled sequence of enzymes (Figure 1), whereby the glutamate product of BCATm activity was re-oxidised to  $\alpha$ -keto glutarate along with hydrogen peroxide by the enzyme glutamate oxidase. The peroxide thus generated was detected by reaction with 1-(3,7-dihydroxy-10H-phenoxazin-10-yl)ethanone to form resorufin, catalysed by the enzyme horseradish peroxidase. Decoupled parallel control wells, without the BCATm initiated step were added to detect any inhibitors of the coupled processes. A potential risk of carrying out fragment screening using such a coupled enzyme system was that genuine inhibitors of BCATm could be discarded as non-specific in nature due the higher chances of fragments interacting with more than one

enzyme. Theoretical reasoning based on complexity,<sup>13</sup> on which much of FBDD methodology is predicated, suggest that there is a higher probability of smaller molecules binding to any given protein than for larger molecules. Therefore, it is more likely that fragments binding to BCATm may also bind to the coupled enzyme glutamate oxidase than would be the case if this assay was used for a traditional HTS campaign with larger, more complex molecules. However, using this functional biochemical assay had the advantage that all biochemical forms of the protein necessary for reaction could be sampled, permitting the detection of inhibitors that inhibited only one of these forms.

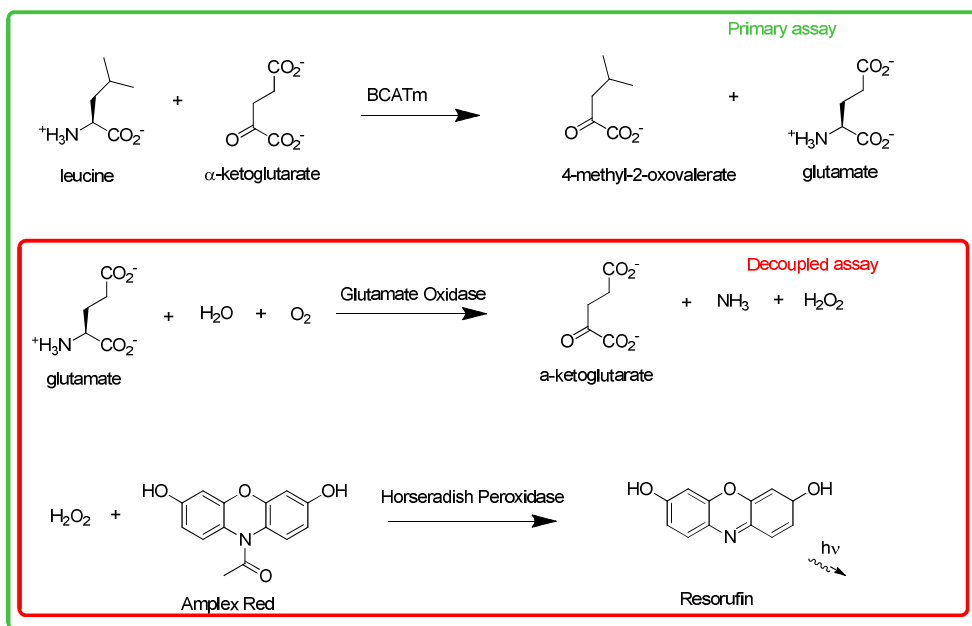


**Figure 1: Biochemical assay format**

As is common in fragment screening campaigns, complementary biophysical screening was also carried out to detect compounds which bound to BCATm; in this case NMR and thermal shift techniques were used. The saturation transfer difference (STD) NMR assay<sup>14</sup> used a mixture of the PLP and PMP forms of the enzyme. Hits identified may interact with either, or potentially

1  
2  
3 both, the PLP and PMP forms of the protein. However, as both forms are catalytically relevant  
4  
5 the precise binding profile was not initially determined as all hits had the potential to yield  
6  
7 functional inhibitors. The STD-NMR approach was complemented by a thermal shift screen  
8  
9 ( $T_m$ ),<sup>15</sup> where both forms of the enzyme were independently assayed. This was necessary  
10  
11 because of the very different denaturation temperatures of the PLP(E) and PMP(F) bound  
12  
13 proteins, 73 °C and 54 °C, respectively.  
14  
15  
16  
17

18  
19 The GSK core fragment library of 1056 compounds was screened in parallel through all three  
20  
21 assays and hit rates are shown in **Figure 2**. The crystallography was carried out by soaking high  
22  
23 concentration solutions (40 - 60 mM) of the ligand of interest into preformed crystals of both  
24  
25 PMP and PLP forms of the protein for one to fourteen days, sometimes yielding liganded crystals  
26  
27 that gave datasets sufficient to unambiguously determine binding modes (resolutions in the range  
28  
29 1.8 - 2.4 Å). Although crystals of both the PLP and PMP forms of the BCATm were tried, the  
30  
31 initial hits only yielded complexes with the more stable PLP protein. We therefore took the  
32  
33 pragmatic decision to prioritise inhibitors for which crystal structures could be elucidated,  
34  
35 thereby concentrating efforts on inhibitors of the PLP form of BCATm.  
36  
37  
38  
39  
40  
41  
42  
43  
44  
45  
46  
47  
48  
49  
50  
51  
52  
53  
54  
55  
56  
57  
58  
59  
60



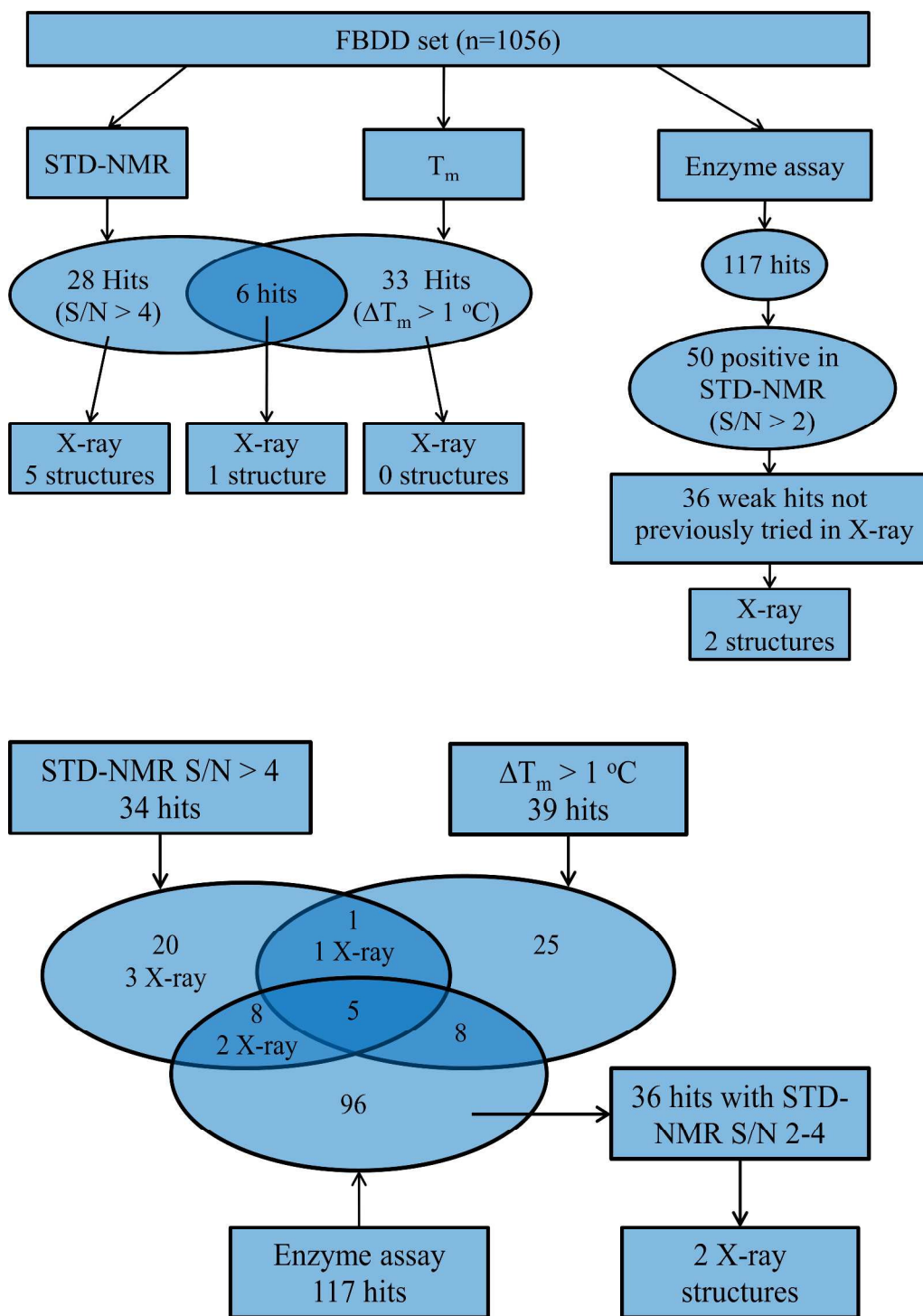


**Figure 2: Flow and Venn diagrams illustrating the output of the fragment screening campaign, showing number of hits identified by each screening technique and the logic**

1  
2  
3 **employed for X-ray prioritisation, plus the distribution of those which yielded X-ray**  
4 **crystal structures.**  
5  
6  
7

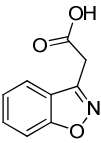
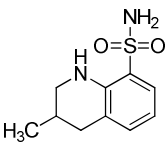
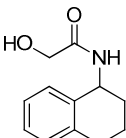
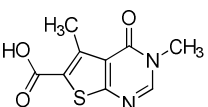
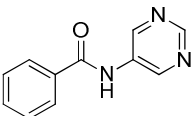
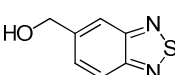
8  
9 The output of the fragment screening is summarised in Figure 2. The different screening  
10 techniques produced different sets of hits, which is a common observation in FBDD campaigns<sup>8</sup>,  
11 as screening is carried out close to the limits of detection for the assays and different  
12 experimental conditions may favour a particular target conformation. All of the hits from either  
13 of the biophysical assays were progressed to X-ray crystallography. The STD-NMR experiment  
14 gave the better success rate in identifying apparent binders that led to liganded X-ray structures,  
15 with the orthogonal thermal shift experiment showing a relatively poor prediction of success.  
16 The biochemical assay had yielded a high number of specific hits, which could not all be  
17 progressed to crystallography, so the STD-NMR data was used to triage these hits, using a lower  
18 cut-off ( $2 \times$  signal to noise, versus  $4 \times$  signal to noise) than was used in the initial selection of  
19 NMR hits.  
20  
21  
22  
23  
24  
25  
26  
27  
28  
29  
30  
31  
32  
33  
34  
35

36 Additional activities were carried out in an effort to increase the number of liganded X-ray  
37 structures as potential starting points for chemical optimisation. Five compounds identified were  
38 hits in both  $T_m$  and NMR assays but failed to produce crystal structures. Given reasonable  
39 confidence that these compounds were genuinely binding to BCAT<sub>m</sub>, structural analogues were  
40 sourced from the GSK compound collection and screened in the STD-NMR and biochemical  
41 assays. Analogue searching was performed by focussed substructure searching complemented by  
42 a GSK-developed workflow, *FindAnalogues*, specifically designed for fragment follow-up.  
43 *FindAnalogues* combines substructure and similarity searching methods with different  
44 descriptors and constraints on compound properties to identify suitable fragment like analogues  
45 from both in-house and external vendors (see Experimental for details). 80 compounds were  
46  
47  
48  
49  
50  
51  
52  
53  
54  
55  
56  
57  
58  
59  
60

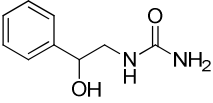
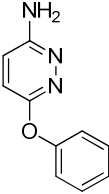
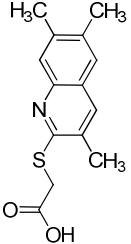
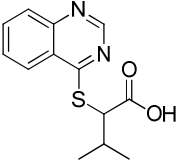
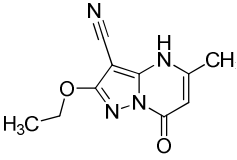
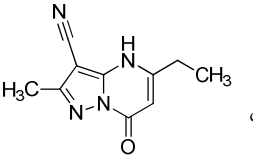
1  
2  
3 selected from this exercise and screened. 32 compounds were identified with activity in one of  
4  
5 the two assays, from which three yielded liganded structures where the original fragment hit had  
6  
7 not (**12**, **13**, **15**). An additional 120 similarly selected analogues were subsequently screened and  
8  
9 yielded valuable SAR for compounds **4** and **5** as described below.  
10  
11

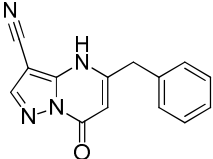
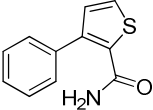
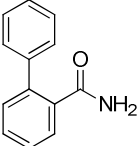
12  
13  
14 Concurrent with this fragment screen, a high throughput screen of the GSK HTS compound  
15  
16 collection (1.7 million compounds) had been conducted. The single-shot percentage inhibition  
17  
18 data and subsequent  $XC_{50}$  data were interrogated for compounds that were identified by the  
19  
20 *FindAnalogues* search. Four analogues of **1** were identified with micromolar activity in the HTS  
21  
22 and were submitted to crystallography, yielding additional liganded structures **9** and **10**.  
23  
24  
25  
26  
27  
28  
29  
30  
31  
32  
33  
34  
35  
36  
37  
38  
39  
40  
41  
42  
43  
44  
45  
46  
47  
48  
49  
50  
51  
52  
53  
54  
55  
56  
57  
58  
59  
60

## Fragment Hits

Compound Number	Structure	pIC <sub>50</sub>	clogP	Heavy Atoms	LE	LLE <sub>AT</sub>	Source	Binding Mode
1		<2.9	0.78	13			STD-NMR	PLP lipophilic pocket, Hydrogen bond acceptor to Ala-314
2		<2.9	1.25	15			T <sub>m</sub> and STD-NMR	PLP lipophilic pocket, Hydrogen bond acceptor to Ala-314
3		<2.9	1.57	15			STD-NMR	PLP lipophilic pocket, Hydrogen bond acceptor to Ala-314
4		4.2 <sup>a</sup>	0.62	15	0.38	0.43	STD-NMR and biochemical	π-stacking to Phe-30, Hydrogen bond acceptor to Lys-79
5		3.0 <sup>b</sup>	1.31	15	0.27	0.26	STD-NMR and biochemical	π-stacking to Phe-30, PLP lipophilic pocket
6		<2.9	1.96	11			STD-NMR	Interface between protein dimers (no functional effect)

1  
2  
3  
4  
5  
6  
7  
8  
9  
10  
11  
12  
13  
14  
15  
16  
17  
18  
19  
20  
21  
22  
23  
24  
25  
26  
27  
28  
29  
30  
31  
32  
33  
34  
35  
36  
37  
38  
39  
40  
41  
42  
43  
44  
45  
46  
47  
48  
49  
50  
51  
52  
53  
54  
55  
56  
57  
58  
59  
60

7		3.1	-0.2	13	0.33	0.45	STD-NMR and biochemical	PLP lipophilic pocket, Hydrogen bond acceptor to Ala-314, Displacement of water adjacent to Cys-315
8		3.9	1.6	14	0.38	0.33	STD-NMR and biochemical	$\pi$ -stacking to Phe-30, PLP lipophilic pocket
9		6.6	3.8	18	0.48	0.30	HTS hit with similarity to fragment hits	Hydrogen bond acceptor to Ala-314
10		5.1	2.69	18	0.39	0.29	HTS hit with similarity to fragment hits	$\pi$ -stacking to Phe-30
11		3.3 <sup>c</sup>	0.21	16	0.28	0.41	T <sub>m</sub> , STD- NMR and biochemical	No crystal structure obtained
12		<3.2 <sup>d</sup>	0.14	15	0.40	0.50	Analogue of <b>11</b>	PLP lipophilic pocket, Displacement of water adjacent to Cys-315

13		4.6	0.77	19	0.44	0.45	Analogue of <b>11</b>	PLP lipophilic pocket, Displacement of water adjacent to Cys-315
14		3.8	1.9	14	0.37	0.29	T <sub>m</sub> , STD-NMR and biochemical	No crystal structure obtained
15		3.8	2.08	15	0.35	0.26	Analogue of <b>14</b>	PLP lipophilic pocket, Hydrogen bond acceptor to Ala-314

**Table 1 Summary of fragment hits identified.** <sup>a</sup> compound reported inactive ( $pIC_{50} < 4.2$ ) on 3 out of 35 test occasions; <sup>b</sup> compound reported inactive ( $pIC_{50} < 2.9$ ) on 1 out of 2 test occasions; <sup>c</sup> compound reported inactive ( $pIC_{50} < 2.9$ ) on 1 out of 3 test occasions; <sup>d</sup> compound reported inactive ( $pIC_{50} < 3.2$ ) on 2 out of 4 test occasions.

**Table 1** summarises the fragment hits identified which yielded liganded crystal structures, along with their calculated ligand efficiency (LE)<sup>16</sup> and modified lipophilic ligand efficiency (LLE<sub>AT</sub>) as defined by researchers at Astex.<sup>17</sup> The crystal structures obtained for the hits, showed occupation of a range of positions in the BCAT<sub>m</sub> binding site, and that significant movement in the protein was induced by the compounds. Some of the most important features for binding are summarised in the X-ray crystal structures shown in **Figure 3**.

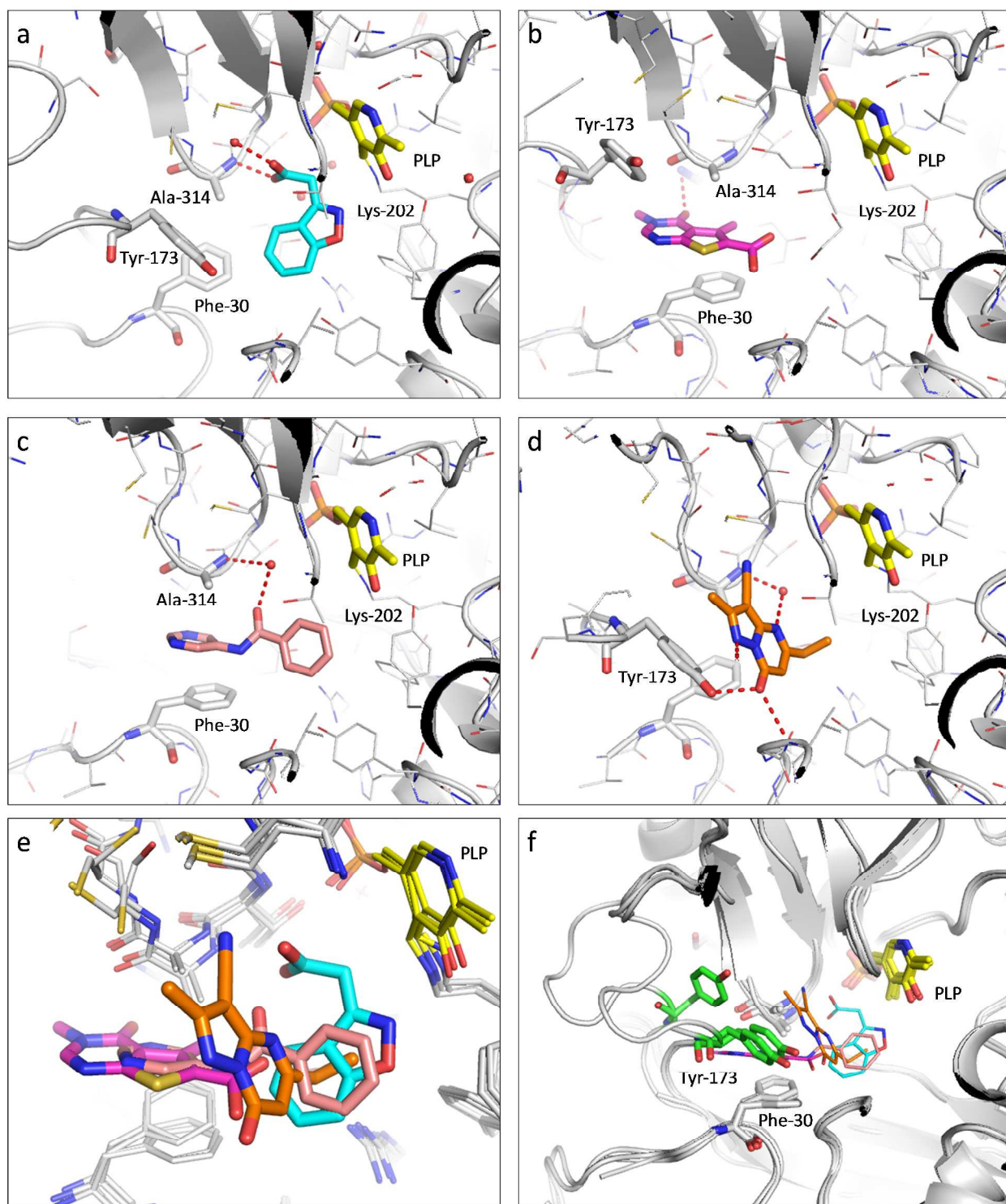


**Figure 3: X-ray crystal structures of compounds 1(cyan, PDB entry 5I5S), 4(magenta PDB entry 5I5V), 5(pink PDB entry 5I5W) and 12(orange PDB entry 5BWT<sup>4</sup>) in the**

1  
2  
3 **BCATm binding site in panels a, b, c and d respectively. Panel e shows an overlay of all**  
4 **these compounds within the binding site. Panel f shows the same overlay but with Tyr-173**  
5 **in green stick format, highlighting the mobility of the 170-180 loop region.**  
6  
7  
8  
9

10  
11 Benzo[*d*]isoxazole **1 (Figure 3a)** occupied a binding pocket defined by a lipophilic region  
12 adjacent to the PLP cofactor, which is confined by a closed ‘gate’ between residues Phe-30 and  
13 Tyr-173. The carboxylic acid carbonyl group acted as a hydrogen bond acceptor to the backbone  
14 NH of Ala-314.  
15  
16  
17  
18  
19

20  
21 The crystal structure of thienopyrimidine **4 (Figure 3b)** showed occupation of a distinct  
22 binding site. The site adjacent to the cofactor was occupied only by ethylene glycol (present in  
23 crystallography medium) and the Phe-30 Tyr-173 ‘gate’ had opened to allow the formation of a  
24  $\pi$ -stacking interaction between Phe-30 and the heterocyclic core. The opening of the gate  
25 involved significant conformational rearrangement, with Phe-30 moving by around 2 Å, whilst  
26 Tyr-173 moved by approximately 6 Å. Additionally, the amide carbonyl acted as a hydrogen  
27 bond acceptor to a lysine NH (Lys-79).  
28  
29  
30  
31  
32  
33  
34  
35  
36  
37  
38

39 The pyrimidine ring of the biaryl amide **5 (Figure 3c)** formed a similar  $\pi$ -stacking interaction  
40 with Phe-30 to thienopyrimidine **4**, whilst the phenyl ring occupied a similar lipophilic aromatic  
41 pocket to benzo[*d*]isoxazole **1**. The tyrosine residue, which moved to open the induced pocket in  
42 the structure of **4** (Tyr-173) was completely disordered in this structure. There are no direct  
43 hydrogen bonding interactions between the heteroatoms of the fragment and the protein, which  
44 may explain the poor ligand efficiency observed. However the amide carbonyl is well solvated  
45 and there is a water mediated hydrogen bond to the hydroxyl of Tyr-141. Biaryl amide **5** was an  
46  
47  
48  
49  
50  
51  
52  
53  
54  
55  
56  
57  
58  
59  
60



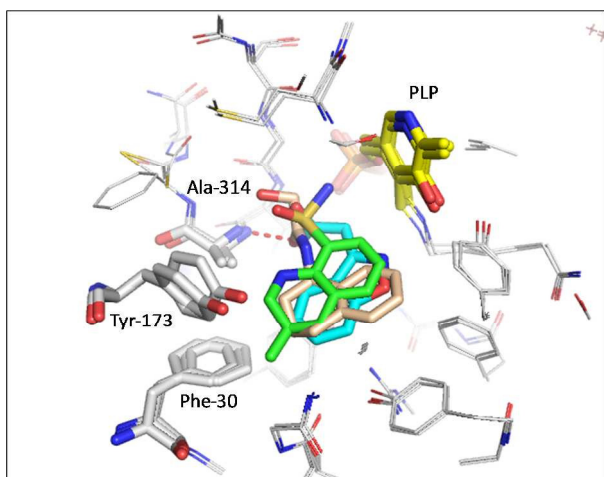
1  
2  
3 effective bridge between the two binding sites identified, and demonstrated that it is possible to  
4  
5 have both sites occupied simultaneously.  
6  
7

8  
9 Pyrazolopyrimidine **12** (**Figure 3d** PDB entry 5BWT<sup>4</sup>) displayed an additional distinct binding  
10  
11 mode. The pendant ethyl group was close to the lipophilic site occupied by aromatic groups for  
12  
13 compounds **1** and **5**, and the ‘gate’ was closed. The heterocyclic core was positioned in a site  
14  
15 which was unoccupied in the other structures, with the nitrile substituent displacing a water  
16  
17 molecule, which formed a hydrogen bonding interaction with the NH of Cys-315 in other  
18  
19 structures. The pyridone carbonyl forms hydrogen bonds with Tyr-173 and the backbone of Val-  
20  
21 155. The pyridone NH and pyrazole N are both involved in water networks.  
22  
23  
24

25  
26  
27 When all of these liganded crystal structures of the fragment hits were considered together  
28  
29 (**Figure 3e and f**), it was clear that the BCAT<sub>m</sub> protein has considerable flexibility to  
30  
31 accommodate a range of ligand binding modes. However, there were several binding ‘hot-spots’  
32  
33 identified, which appeared to act as anchors for the fragments. The most notable of these was the  
34  
35 lipophilic pocket adjacent to the PLP, hydrogen bonding with Ala-314,  $\pi$ -stacking with Phe-30  
36  
37 and displacement of the water molecule adjacent to Cys-315. All of the hits identified satisfied at  
38  
39 least one of these interactions (see **Table 1**). This flexibility in the protein would thus have  
40  
41 caused difficulties in attempting to predict the binding modes of hits using docking methods  
42  
43 alone. Therefore, to enable structure based fragment growth, it was important to generate  
44  
45 multiple X-ray crystal structures (as is common practice), even for compounds which appeared  
46  
47 to be closely structurally related. The diversity of structural information obtained provided  
48  
49 opportunities to grow the fragment hits in various ways<sup>18</sup>.  
50  
51  
52  
53  
54

## 55 56 **Hits to Leads Optimisation** 57 58 59 60

1  
2  
3 The fragment hits identified were grouped (“clustered”) according to their binding modes in  
4 the BCATm active site. An example of this process is shown for compounds **1**, **2** and **3**, which  
5 look dissimilar on the basis of their chemical structures, but which all make similar binding  
6 interactions with the protein (**Figure 4**). One exemplar was chosen from each vectorial cluster,  
7 either because it demonstrated superior efficiency of binding, or because it offered more flexible  
8 and tractable chemistry than other structures within the same cluster. The fragment growth and  
9 further optimisation of the pyrazolopyrimidinone series represented by compounds **11-13** is  
10 described in the complementary paper;<sup>4</sup> a noteworthy feature of this series was that the original  
11 fragment hit (**11**) did not give a crystal structure, but analogue searching identified closely  
12 related compounds that did yield liganded crystal structures. Herein, the initial lead optimisation  
13 efforts on two other series to illustrate the strategies employed are described.  
14  
15  
16  
17  
18  
19  
20  
21  
22  
23  
24  
25  
26  
27  
28  
29



30  
31  
32  
33  
34  
35  
36  
37  
38  
39  
40  
41  
42  
43  
44  
45  
46  
47  
48 **Figure 4: Example of vectorial clustering, showing an overlay of compounds 1 (cyan PDB**  
49 **entry 5I5S), 2(green PDB entry 5I5T) and 3(beige PDB entry 5I5U) with similar binding**  
50 **interactions.**  
51  
52  
53  
54  
55  
56  
57  
58  
59  
60

1  
2  
3 Thienopyrimidine **4** had very favourable LE and LLE<sub>AT</sub> values and contained a tractable  
4 functional group (carboxylic acid), which could be used to grow towards the PLP pocket. The  
5  
6 crystal structure of biaryl amide **5** provided further confidence in this approach because it  
7  
8 showed that concomitant binding in both of these pockets could be achieved. With these aims in  
9  
10 mind, initial optimisation focussed on a small array of amides, mostly containing lipophilic  
11  
12 substituents, which were designed to fill the PLP pocket.  
13  
14  
15  
16  
17

18 These compounds were synthesised using HATU-mediated coupling chemistry or *via* acylation  
19 using the appropriate acid chloride (**Table 2**). Due to monomer availability, some of the  
20  
21 chemistry was carried out on the closely related des-methyl series e.g. **16**, which showed similar  
22  
23 activity to the initial hit **4**. Analogues **17** and **18** confirmed that activity with either of these two  
24  
25 substituents was comparable. In general, aromatic amides were preferred to aliphatic  
26  
27 substituents, as demonstrated by the comparisons between compounds **17** and **18** plus **19** and **20**.  
28  
29 Substitution on the pendant phenyl ring was only tolerated in the *ortho* position (compounds **21**,  
30  
31 **22**, **23**). Attempts to accommodate heteroaromatic rings in the lipophilic pocket were not  
32  
33 productive (e.g. compounds **24** and **25**), with the exceptions of the lipophilic thiophene (**26**) and  
34  
35 thiadiazole (**27**), both of which also maintained the highly favourable LE and LLE<sub>AT</sub> values of  
36  
37 the hit.  
38  
39  
40  
41  
42  
43  
44  
45  
46  
47  
48  
49  
50  
51  
52  
53  
54  
55  
56  
57  
58  
59  
60

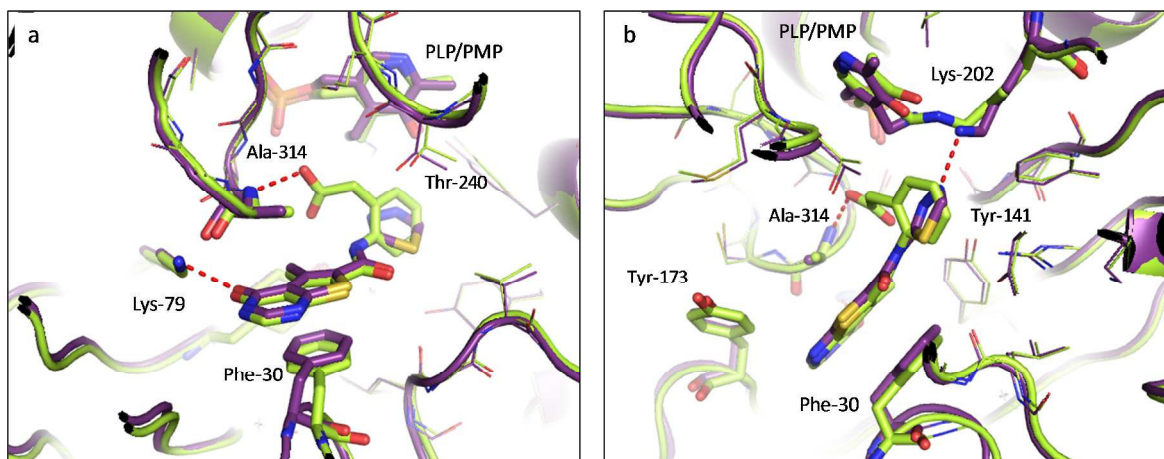
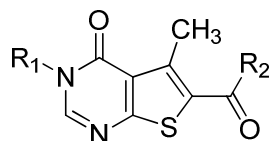


**Figure 5: Overlay of compounds 27 (purple PDB entry 5I5X) and 29 (pale green PDB entry 5I5Y). Panel a. shows the common interactions with Lys-79, Phe-30 and Ala-314. Panel b. illustrates the difference in interactions around PLP/PMP for the two compounds**

The potency associated with compound **27** could not be rationalised by knowledge of the crystal structure of compound **4**. Soaking experiments failed to produce a crystal structure of compound **27**, however co-crystallisation was successful, which yielded the first liganded structure of BCATm in the PMP form (**Figure 5**). The PMP form shows a few significant differences with respect to the PLP form. Firstly, the Lys-202 sidechain, now no longer covalently linked to cofactor, as in the PLP form, is free to shift slightly to optimally interact with one of the nitrogen atoms in the thiadiazole ring. Secondly, the PMP cofactor pyridine rotates by  $\sim 11^\circ$  from the PLP pyridine plane and Leu-266 adopts a lower energy rotamer conformation due to the additional space created by the rotation of the PMP pyridine ring. Due to its potent inhibition of BCATm, compound **27** was progressed to a cellular assay measuring BCATm inhibition, and was found to have a cellular  $pIC_{50}$  value of 5.4.



Compound Number	R1	R2	pIC <sub>50</sub>	LE	LLE <sub>AT</sub>
4	CH <sub>3</sub>	OH	4.2 <sup>a</sup>	0.38	0.44
16	H	OH	4.3	0.44	0.51
17	CH <sub>3</sub>		5.1	0.33	0.34
18	H		5.1	0.36	0.37
19	CH <sub>3</sub>		< 4.2		
20	CH <sub>3</sub>		< 3.2		
21	H		4.3 <sup>b</sup>	0.28	0.30

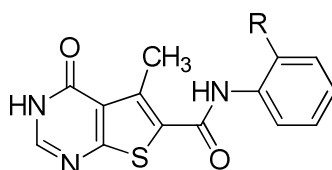
22	H		< 4.2		
23	H		< 4.2		
24	H		3.6	0.25	0.33
25	H		< 4.2		
26	H		5.8	0.48	0.45
27	H		6.7	0.48	0.63

**Table 2: Activity and efficiency data for amide analogues of compound 4.**

<sup>a</sup> compound reported inactive ( $pIC_{50} < 4.2$ ) on 3 out of 35 test occasions; <sup>b</sup> compound reported inactive ( $pIC_{50} < 4.2$ ) on 2 out of 4 test occasions.

The next logical expansion was to grow towards Ala-314 to try to exploit a hydrogen-bonding opportunity, which had been identified from the fragment screening as a binding hot-spot. A

range of heteroatom-containing functional groups were introduced in the *ortho*-position of compound **18** (Table ). From this effort, only the aryl acetate **29** showed any significant improvement in BCATm inhibition resulting in micromolar activity, whilst maintaining good efficiencies. Crystallisation of this compound in BCATm (Figure 5) confirmed that the acid carbonyl moiety was acting as a hydrogen bond acceptor to the backbone NH of Ala-314.



Compound Number	R	pIC <sub>50</sub>	LE	LLE <sub>AT</sub>
<b>18</b>	H	5.1	0.36	0.37
<b>28</b>		< 4.2		
<b>29</b>		6.0	0.34	0.45
<b>30</b>		5.0	0.31	0.44
<b>31</b>		4.9	0.28	0.41

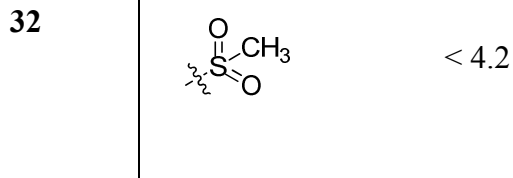


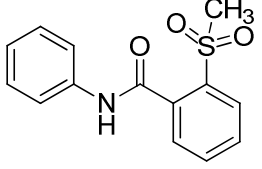
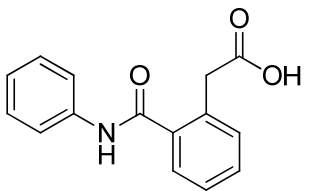
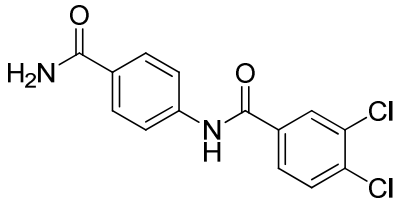
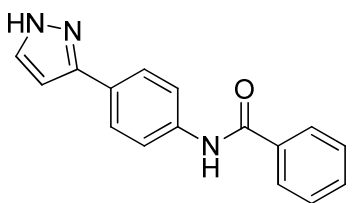
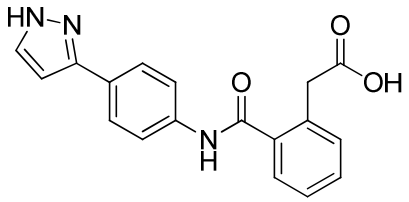
**Table 3: Results of targeting Ala-314 through growth from the *ortho*-position of 18**

By using the structural information obtained from different fragment hits to identify binding hot spots it was thus possible to grow weakly active fragment **4** into more potent analogues, with activity in a cellular assay.

Analysis of structures showed that biaryl amide **5** offered potential vectors towards the Ala-314 NH donor and the Lys-79 NH<sub>2</sub> donor, to which the pyrimidinone carbonyl of **4** was hydrogen bonded. The biaryl amide substructure is an abundant motif in the GSK compound collection, so the initial SAR was readily delineated (**Table 4**).

Compound	Structure	pIC <sub>50</sub>	LE	LLE <sub>AT</sub>	clogP
<b>5</b>		3.0	0.27	0.26	1.31
<b>33</b>		< 3.2			2.65

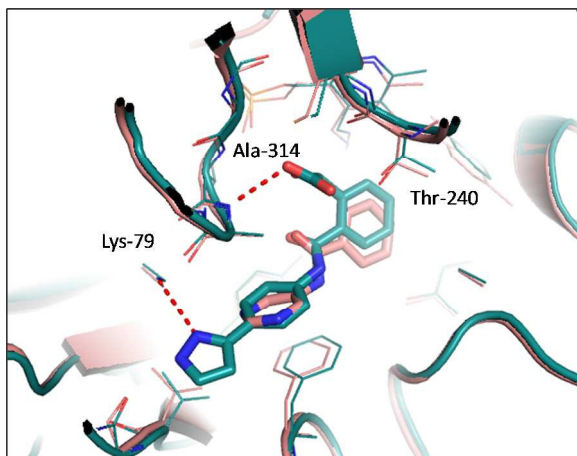


34		3.7	0.27	0.26	1.66
35		3.5 <sup>a</sup>	0.25	0.25	1.58
36		5.6	0.39	0.31	2.86
37		5.3	0.36	0.26	3.00
38		5.7	0.33	0.32	1.94

**Table 4: Screening results from analogues of 5 available in the GSK collection.**

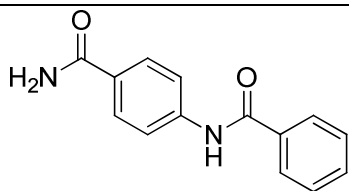
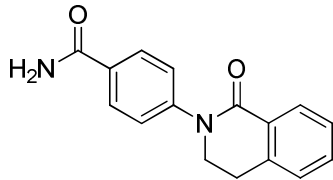
<sup>a</sup> compound reported inactive ( $pIC_{50} < 4.2$ ) on 2 out of 4 test occasions.

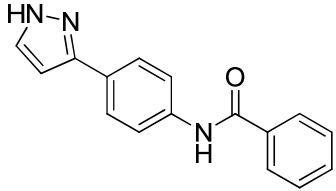
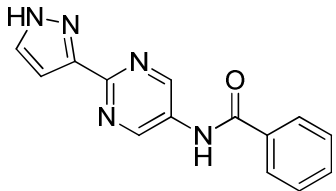
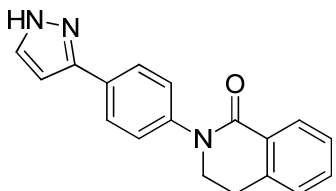
1  
2  
3 The pyrimidine ring was initially replaced with phenyl, as a greater number of analogues were  
4 available, and the crystal structure of **5** suggested that the pyrimidine nitrogens were not  
5 participating in any binding interactions. As with the optimisation of **4**, it was found that adding  
6 hydrogen bond acceptors, which could interact with Ala-314, provided modest improvements in  
7 binding (**34** and **35**), with maintained ligand efficiency. A more dramatic improvement in  
8 enzyme inhibition was achieved when hydrogen bond acceptors, represented by carboxamide  
9 and pyrazole (**36** and **37**), enabled engagement with Lys-79. Carboxamide **36** also had additional  
10 lipophilic chlorine groups that enhanced binding in the PLP pocket, contributing to micromolar  
11 levels of activity, which represented a roughly 1000-fold increase in activity from the fragment  
12 hit. This compound also displayed a significant improvement in the efficiency measures relative  
13 to the hit compound **5**. Synthesis of compound **38**, which combined the acceptors targeting both  
14 Lys-79 and Ala-314 demonstrated that the effects on the activity could be additive, with good LE  
15 and  $LLE_{AT}$  values achieved. The intent of this design was confirmed by the Xray structure of **38**  
16 within BCATm shown in **Figure 6**.  
17  
18  
19  
20  
21  
22  
23  
24  
25  
26  
27  
28  
29  
30  
31  
32  
33  
34  
35



53  
54 **Figure 6: Overlay of compounds 38 (blue PDB entry 5I60) and 5 (pink PDB entry 5I5W)**  
55 **confirms 38 makes additional interactions with Lys-79 and Ala-314.**  
56  
57  
58  
59  
60

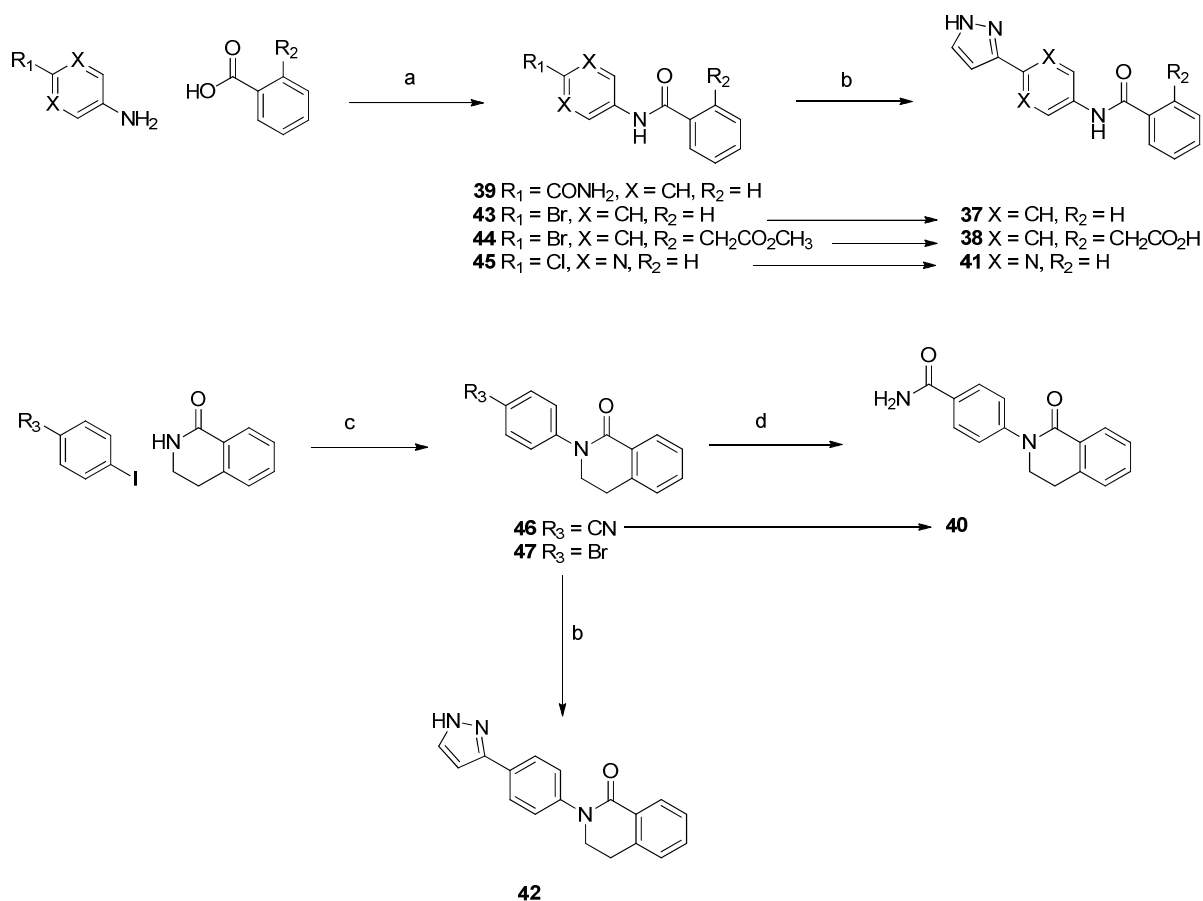
Once a good understanding of the SAR within this series had been established through screening of available analogues, attention was turned to improving the physicochemical profiles of the compounds. Biaryl amides are notoriously insoluble, being highly planar and crystalline,<sup>19</sup> and indeed, the measured solubilities of these compounds were poor (**Table** , compounds **37** and **39**). Two strategies were adopted to improve the solubility within the series. The amide N-H was constrained in a tetrahydroisoquinoline ring to prevent intermolecular hydrogen bonding, which could contribute to the high crystallinity (**40** and **42**). Additionally, the pyrimidine ring from the initial hit was returned to the molecules in place of the phenyl ring to lower the lipophilicity (compound **41**). The targeted analogues were synthesised as shown in **Scheme 2**. Both of these strategies resulted in a modest improvement in enzyme inhibition and approximately 10-fold increased solubility. As in the optimisation of thienopyrimidine **4**, the biaryl amide series had been grown into a series of lead-like molecules through focussed structure-based design combined with consideration of molecular properties.

Compound	Structure	pIC <sub>50</sub>	LE	LLE <sub>AT</sub>	clogP	Sol(μg/ml)
<b>39</b>		4.3 <sup>a</sup>	0.33	0.33	1.46	13
<b>40</b>		4.8	0.33	0.36	1.14	132

1							
2							
3							
4							
5	37		5.2	0.36	0.26	3.00	12
6							
7							
8							
9							
10							
11							
12	41		5.5	0.38	0.35	1.94	82
13							
14							
15							
16							
17							
18							
19							
20							
21	42		5.8	0.36	0.29	2.83	94
22							
23							
24							
25							
26							
27							
28							
29							
30							
31							

**Table 5: Data from the biaryl amides series, illustrating structural modifications**

**designed to improve solubility.** <sup>a</sup> compound reported inactive ( $pIC_{50} < 4.2$ ) on 1 out of 4 test occasions



Reagents and conditions: (a) HATU, DIPEA, DMF, 20 – 40 °C, 41-79 %; (b) 1*H*-pyrazol-3-ylboronic acid, Pd(PPh<sub>3</sub>)<sub>4</sub>, Na<sub>2</sub>CO<sub>3</sub> (sat. aq.), 130 °C, microwave 20 min. 41 – 72 %; (c) CuI, K<sub>2</sub>CO<sub>3</sub>, DMF, 160 °C, 18 h, 57 – 66%; (d) 2M NaOH (aq.), 30 % H<sub>2</sub>O<sub>2</sub> (aq.), EtOH, 50 °C, 20 h, 19 %.

## Scheme 2: Synthesis of analogues of compound 5

### Conclusions

When carrying out any diversity screening campaign, but particularly when utilising fragment-based approaches, it is important to realise that different biochemical and biophysical screening techniques can, and indeed do, identify different sub-sets of hits. Therefore, there could be an

1  
2  
3 advantage to using multiple, complementary techniques for the initial screening phase. This is  
4 particularly important in FBDD, where the binding of hits will likely to be near to the limit of  
5 detection in some assays. This set of hits identified for BCATm, and the crystal structures  
6 generated have illustrated many aspects of the binding of small molecules to this enzyme for the  
7 first time. It was particularly interesting to observe such different conformations of the protein  
8 between different fragment hits, whilst gratifying to be able to identify several binding ‘hot  
9 spots’ in the protein structure and confirm that these could be accessed simultaneously and from  
10 different structural types. The insights from multiple liganded crystal structures during both the  
11 screening and chemical optimisation stages were invaluable in guiding progress, consistent with  
12 contemporary practice<sup>11,20</sup> in fragment based design. Another important aspect of this work was  
13 the use of analogue searching from an extensive collection. This was important both in the hit  
14 finding phase, where it was used to generate additional hits, and in fragment optimisation and  
15 growth, where significant improvements in hit activities were obtained without recourse to  
16 synthesis. The chemical libraries are a major asset for large pharmaceutical companies, which  
17 allow scientists to rapidly explore SAR around fragment hits. The “SAR by catalogue” allowed  
18 expansion beyond the deliberately designed screening sets, whilst continuing to exercise  
19 discipline with the molecular properties of compounds screened. Finally, micromolar inhibitors  
20 of BCATm have been identified, with characterised novel binding modes and measurable  
21 activities in a cellular assay. This represents a major step forward towards the goal of  
22 establishing if pharmaceutical inhibition of BCATm using small molecules could provide a  
23 useful treatment for metabolic diseases; the accompanying paper<sup>4</sup> describes further progress  
24 achieved in one series.

## 55 56 **Experimental** 57 58 59 60

## Chemistry

All solvents and reagents, unless otherwise stated, were commercially available from regular suppliers such as Sigma-Aldrich and Fluorochem and were used as purchased without further purification. Nuclear magnetic resonance ( $^1\text{H}$  NMR and  $^{13}\text{C}$  NMR) spectra were recorded on a Bruker AVI (400 MHz), Bruker Nano (500 MHz) or Bruker AVII+ (600 MHz) spectrometer (with cryoprobe) in the indicated solvent. Chemical shifts  $\delta$  are reported in parts per million (ppm) relative to tetramethylsilane and are internally referenced to the residual solvent peak. Coupling constants ( $J$ ) are given in Hertz (Hz) to the nearest 0.5 Hz. Liquid Chromatography Mass Spectroscopy (LCMS) analysis was conducted on either System A, a Waters Acquity UPLC BEH  $\text{C}_{18}$  column (50 mm x 2.1 mm i.d. 1.7  $\mu\text{m}$  packing diameter) at 40  $^\circ\text{C}$  eluting with 0.1 % v/v solution of formic acid in water (solvent A) and 0.1 % v/v solution of formic acid in acetonitrile (solvent B), using the following elution gradient 0.0-1.5 min 3-100% B, 1.5-1.9 min 100% B, 1.9-2.0 min 3% B, at a flow rate of 1 mL/min; or System B, a Waters Acquity UPLC BEH  $\text{C}_{18}$  column (50 mm x 2.1 mm i.d. 1.7  $\mu\text{m}$  packing diameter) at 40  $^\circ\text{C}$  eluting with 10 mM ammonium bicarbonate in water adjusted to pH 10 with ammonia solution (solvent A) and acetonitrile (solvent B), using the following elution gradient 0.0-1.5 min 1-97% B, 1.5-1.9 min 97% B, 1.9-2.0 min 100% B, at a flow rate of 1 mL/min. The UV detection was based on an average signal from wavelength of 210 nm to 350 nm. The mass spectra were recorded on a Waters ZQ mass spectrometer using alternate-scan positive and negative mode electrospray ionisation. Preparative HPLC using a Mass Directed Auto Purification (MDAP) were conducted on a Waters *FractionLynx* system comprising of a Waters 515 pump with extended pump heads, Waters 2767 auto sampler, Waters 996 photodiode array detector and Gilson 202 fraction collector on an XBridge or Sunfire  $\text{C}_{18}$  column (30 mm x 150 mm i.d. 5 $\mu\text{m}$  packing diameter) at

1  
2  
3 ambient temperature. The mobile phase was 0.1 % v/v solution formic acid in water or 10 mM  
4 ammonium bicarbonate in water adjusted to pH 10 with ammonia solution (solvent A) and 0.1 %  
5 v/v solution formic acid in acetonitrile or acetonitrile (solvent B). The UV detection is a summed  
6 signal from wavelength of 210 nm to 350 nm. The mass spectra were recorded on Waters ZQ  
7 mass spectrometer using alternate-scan positive and negative electrospray ionisation. The  
8 software used was *MassLynx* 3.5 with *OpenLynx* and *FractionLynx* options. High resolution  
9 mass spectra (HRMS) were obtained on a Micromass Q-ToF Ultima hybrid quadrupole time-of-  
10 flight mass spectrometer, equipped with a Z-spray interface (ESI), over a mass range of 100 –  
11 1100 Da, with a scan time of 0.9 s and an interscan delay of 0.1 s. Reserpine was used as the  
12 external mass calibrant ( $[M+H]^+ = 609.2812$  Da). The Q-ToF Ultima mass spectrometer was  
13 operated in W reflectron mode to give a resolution (FWHM) of 16000-20000. Ionisation was  
14 achieved with a spray voltage of 3.2 kV, a cone voltage of 50 V, with cone and desolvation gas  
15 flows of 10-20 and 600 L/hr, respectively. The source block and desolvation temperatures were  
16 maintained at 120 °C and 250 °C respectively. The elemental composition was calculated using  
17 *MassLynx* v4.1 for the  $[M+H]^+$  and the mass error quoted as ppm. Flash column chromatography  
18 was conducted on a Combiflash® Rf, automated flash chromatography system (Teledyne Isco)  
19 using disposable normal or reverse phase Redisep cartridges (4 g to 330 g). The CombiFlash®  
20 Rf used RFID (Radio Frequency Identification Detector) technology to automate setting the  
21 parameters for purification runs and fraction collection. The system was equipped with a UV  
22 variable dual-wavelength and a Foxy® fraction collector enabling automated peak cutting,  
23 collection and tracking. The purity of all compounds screened in the biological assays was  
24 examined by LCMS analysis and was found to be  $\geq 95$  % unless otherwise specified. The human  
25  
26  
27  
28  
29  
30  
31  
32  
33  
34  
35  
36  
37  
38  
39  
40  
41  
42  
43  
44  
45  
46  
47  
48  
49  
50  
51  
52  
53  
54  
55  
56  
57  
58  
59  
60



1  
2  
3 biological samples were sourced ethically and their research use was in accord with the terms of  
4  
5 the informed consents.  
6  
7

8  
9 Compounds **2**, **3**, and **14** were purchased from Enamine. Compound **12** was purchased from  
10 Vitas. Compound **18** was purchased from ChemDiv. Compounds **1**, **4**, **5**, **6**, **7**, **8**, **10**, **13**, **15**, **33**,  
11 and **34** were obtained from the GSK compound collection, but are also available from  
12 commercial suppliers. Compound **35** was obtained from the GSK compound collection and may  
13 be synthesised according to the procedure described by Azizian and co-workers.<sup>21</sup>  
14  
15  
16  
17  
18  
19

20  
21  
22 *2-Ethoxy-5-methyl-7-oxo-4,7-dihydropyrazolo[1,5-a]pyrimidine-3-carbonitrile (11)* was  
23 obtained from the GSK compound collection. <sup>1</sup>H NMR (500 MHz, DMSO-d<sub>6</sub>) δ ppm 5.78 (s, 1  
24 H), 4.36 (q, *J* = 7.0 Hz, 2 H), 2.47 - 2.52 (m, 1 H), 2.27 (s, 3 H). 1.36 (t, *J* = 7.0 Hz, 3 H); LCMS  
25 (ESI, formic) *m/z* 219.01 [M+H]<sup>+</sup>, *R*<sub>t</sub> = 0.63 min.  
26  
27  
28  
29  
30  
31

32  
33 *5-methyl-4-oxo-3,4-dihydrothieno[2,3-d]pyrimidine-6-carboxylic acid (16)*. Lithium  
34 hydroxide, monohydrate (2.3 g, 55 mmol) was added to a solution of ethyl 5-methyl-4-oxo-3,4-  
35 dihydrothieno[2,3-*d*]pyrimidine-6-carboxylate (4.0 g, 17 mmol) in a mixture of THF (50 mL),  
36 MeOH (25 mL) and water (8 mL). The reaction mixture was stirred at room temperature for 16  
37 h. Lithium hydroxide, monohydrate (1.0 g, 24 mmol) was added and the reaction mixture was  
38 stirred for another 6 h. The reaction mixture was then heated at 40 °C for 24 h. Solvent was  
39 evaporated under reduced pressure. The resulting crude product was dissolved in water and the  
40 mixture was acidified to pH 1 with 2 M aqueous HCl solution. The resulting precipitate was  
41 collected by filtration and dried in a vacuum oven overnight to give the title product as a pale  
42 pink solid (3.5 g, 99 %). <sup>1</sup>H NMR (400 MHz, DMSO-d<sub>6</sub>) δ 13.31 (br. s, 1H), 12.56 (br. s, 1H),  
43  
44  
45  
46  
47  
48  
49  
50  
51  
52  
53  
54  
55  
56  
57  
58  
59  
60

1  
2  
3 8.17 (s, 1H), 2.80 (s, 3H); LCMS (ESI, formic)  $m/z$  211.02  $[M+H]^+$ ,  $R_t$  = 0.45 min; HRMS (ESI)  
4  
5 calcd for  $C_8H_6N_2O_3S+H^+$  211.0177, found 211.0172 (2.95 min).  
6  
7

### 8 9 **General procedure A for amide coupling**

10  
11  
12 The appropriate amine (1.2 eq), HATU (1.2 eq) and DIPEA (2 eq) were added to a solution of  
13 3,5-dimethyl-4-oxo-3,4-dihydrothieno[2,3-*d*]pyrimidine-6-carboxylic acid (**4**) (1 eq) in DMF (4 -  
14  
15 10 mL). The mixture was stirred at room temperature until reaction was complete by LCMS.  
16  
17 Water (50 mL) and EtOAc (50 mL) were added. The aqueous phase was extracted with EtOAc  
18  
19 (2 x 50 mL). The organic layers were combined, passed through a hydrophobic frit and  
20  
21 concentrated to dryness under reduced pressure. The resulting crude product was purified by  
22  
23 reverse phase chromatography to give the desired final product.  
24  
25  
26  
27  
28  
29

### 30 **General procedure B for amide coupling**

31  
32  
33 HATU (1.2 eq) and DIPEA (2 eq) were added to a solution of 5-methyl-4-oxo-3,4-  
34  
35 dihydrothieno[2,3-*d*]pyrimidine-6-carboxylic acid (**16**) (1 eq) in DMF (1.5 – 2.5 mL). The  
36  
37 mixture was stirred at room temperature between 1 to 10 min. The appropriate amine (1.2 eq)  
38  
39 was then added and the reaction mixture was stirred at room temperature until reaction was  
40  
41 complete by LCMS. Solvent was then evaporated under reduced pressure. The resulting crude  
42  
43 product was purified by reverse phase chromatography to give the desired final product.  
44  
45  
46  
47

48  
49 *3,5-dimethyl-4-oxo-N-phenyl-3,4-dihydrothieno[2,3-*d*]pyrimidine-6-carboxamide (17)* was  
50  
51 prepared according to general procedure A using aniline (50  $\mu$ L, 0.54 mmol). The resulting crude  
52  
53 product was purified by reverse phase chromatography using the formic acid MDAP (gradient B  
54  
55 over 15 min) to give the title product as white solid (90 mg, 64 %).  $^1H$  NMR (400 MHz, DMSO-  
56  
57  
58  
59  
60

1  
2  
3 d<sub>6</sub>) δ 10.25 (s, 1H), 8.50 (s, 1H), 7.68 (br. d, *J* = 7.5 Hz, 2H), 7.36 (br. t, *J* = 8.0 Hz, 2H), 7.07 -  
4  
5 7.16 (br. t, *J* = 7.5 Hz, 1H), 3.49 (s, 3H), 2.74 (s, 3H); LCMS (ESI, high pH) *m/z* 300.04  
6  
7  
8 [M+H]<sup>+</sup>, *R*<sub>t</sub> = 0.83 min.  
9

10  
11 *5-methyl-4-oxo-N-phenyl-3,4-dihydrothieno[2,3-d]pyrimidine-6-carboxamide (18)* was  
12 prepared according to general procedure B using aniline (50 μL, 0.54 mmol). The crude product  
13 was purified by reverse phase chromatography (C18 column, 10-40 % CH<sub>3</sub>CN (B) / 10 mM  
14 aqueous ammonium bicarbonate solution (A)) to give the title product as a pale yellow solid (87  
15 mg, 64 %). <sup>1</sup>H NMR (400 MHz, DMSO-d<sub>6</sub>) δ 12.57 (br. s, 1H), 10.20 (s, 1H), 8.18 (s, 1H), 7.68  
16 (d, *J* = 7.5 Hz, 2H), 7.36 (t, *J* = 8.0 Hz, 2H), 7.03 - 7.18 (m, 1H), 2.73 (s, 3H); <sup>13</sup>C NMR (101  
17 MHz, DMSO-d<sub>6</sub>) δ 164.2 (C), 160.6 (C=O), 158.3 (C=O), 147.4 (Ar-CH), 138.5 (C), 136.4 (C),  
18 128.7 (2C, Ar-CH), 127.9 (C), 124.0 (Ar-CH), 123.4 (C), 120.3 (2C, Ar-CH), 15.1 (CH<sub>3</sub>); LCMS  
19 (ESI, high pH) *m/z* 286.01 [M+H]<sup>+</sup>, *R*<sub>t</sub> = 0.72 min; HRMS (ESI) calcd for C<sub>14</sub>H<sub>11</sub>N<sub>3</sub>O<sub>2</sub>S+H<sup>+</sup>  
20 286.0650, found 286.0646 (4.08 min); IR (ATR) cm<sup>-1</sup> 3294, 3062, 3020, 2929, 2866, 1656,  
21 1634, 1595, 1580, 1529.  
22  
23  
24  
25  
26  
27  
28  
29  
30  
31  
32  
33  
34  
35  
36  
37

38 *N-cyclopentyl-3,5-dimethyl-4-oxo-3,4-dihydrothieno[2,3-d]pyrimidine-6-carboxamide (19)*  
39 was prepared according to general procedure A using cyclopentanamine (0.026 mL, 0.268 mmol).  
40 Purification twice by reverse phase chromatography using the formic acid MDAP (gradient B  
41 over 15 min) gave the title product as a white solid (20 mg, 28 %). <sup>1</sup>H NMR (400 MHz, CDCl<sub>3</sub>)  
42 δ 8.03 (s, 1H), 5.82 (d, *J* = 6.5 Hz, 1H), 4.39 (apparent sxt, *J* = 7.0 Hz, 1H), 3.58 (s, 3H), 2.86 (s,  
43 3H), 2.05 - 2.17 (m, 2H), 1.62 - 1.81 (m, 4H), 1.45 - 1.57 (m, 2H); LCMS (ESI, formic) *m/z*  
44 292.09 [M+H]<sup>+</sup>, *R*<sub>t</sub> = 0.78 min.  
45  
46  
47  
48  
49  
50  
51  
52  
53  
54  
55  
56  
57  
58  
59  
60

1  
2  
3  
4  
5  
6  
7  
8  
9  
10  
11  
12  
13  
14  
15  
16  
17  
18  
19  
20  
21  
22  
23  
24  
25  
26  
27  
28  
29  
30  
31  
32  
33  
34  
35  
36  
37  
38  
39  
40  
41  
42  
43  
44  
45  
46  
47  
48  
49  
50  
51  
52  
53  
54  
55  
56  
57  
58  
59  
60

*3,5-dimethyl-6-(piperidine-1-carbonyl)thieno[2,3-d]pyrimidin-4(3H)-one (20)* was prepared according to general procedure A using piperidine (0.04 mL, 0.43 mmol). Purification by reverse phase chromatography using the formic acid MDAP (gradient B over 15 min) gave the title product as a white solid (70 mg, 64 %). <sup>1</sup>H NMR (400 MHz, DMSO-d<sub>6</sub>) δ 8.43 (s, 1H), 3.47 (br. s, 7H), 2.43 (s, 3H), 1.56 - 1.67 (m, 2H), 1.55-1.44 (m, 4H); LCMS (ESI, formic) *m/z* 292.17 [M+H]<sup>+</sup>, R<sub>t</sub> = 0.74 min.

*5-methyl-4-oxo-N-(o-tolyl)-3,4-dihydrothieno[2,3-d]pyrimidine-6-carboxamide (21)* was prepared according to general procedure B using *o*-toluidine (0.4 mL, 0.3 mmol). Purification by reverse phase chromatography using the formic acid MDAP (gradient B over 15 min) gave the title product as yellow solid (32 mg, 37 %). <sup>1</sup>H NMR (400 MHz, DMSO-d<sub>6</sub>) δ 12.55 (br. s, 1H), 9.69 (s, 1H), 8.17 (s, 1H), 7.39 (br. d, *J* = 7.5 Hz, 1H), 7.28 (br. d, *J* = 7.0 Hz, 1H), 7.15 - 7.25 (m, 2H), 2.79 (s, 3H), 2.26 (s, 3H); LCMS (ESI, formic) *m/z* 300.04 [M+H]<sup>+</sup>, R<sub>t</sub> = 0.78 min, purity = 94 %.

*5-methyl-4-oxo-N-(m-tolyl)-3,4-dihydrothieno[2,3-d]pyrimidine-6-carboxamide (22)* was prepared according to general procedure B using *m*-toluidine (60 μL, 0.57 mmol). Purification by reverse phase chromatography using the formic acid MDAP (gradient B over 15 min) gave the title product as a white solid (39 mg, 46 %). <sup>1</sup>H NMR (400 MHz, DMSO-d<sub>6</sub>) δ 12.55 (br. s, 1H), 10.12 (s, 1H), 8.17 (s, 1H), 7.51 (s, 1H), 7.47 (d, *J* = 8.5 Hz, 1H), 7.23 (t, *J* = 8.0 Hz, 1H), 6.94 (d, *J* = 7.5 Hz, 1H), 2.73 (s, 3H), 2.31 (s, 3H); <sup>13</sup>C NMR (101 MHz, DMSO-d<sub>6</sub>) δ 164.2 (C), 160.5 (C=O), 158.3 (C=O), 147.3 (CH), 138.4 (C), 137.9 (C), 136.3(C), 128.5 (C), 128.0 (CH), 124.7 (CH), 123.4 (C), 120.8 (CH), 117.5 (CH), 21.1 (CH<sub>3</sub>), 15.0 (CH<sub>3</sub>); LCMS (ESI, formic) *m/z* 300.11 [M+H]<sup>+</sup>, R<sub>t</sub> = 0.85 min; HRMS (ESI) calcd for C<sub>15</sub>H<sub>13</sub>N<sub>3</sub>O<sub>2</sub>S+H<sup>+</sup> 300.0801, found 300.0798 (4.21 min).

1  
2  
3  
4  
5  
6  
7  
8  
9  
10  
11  
12  
13  
14  
15  
16  
17  
18  
19  
20  
21  
22  
23  
24  
25  
26  
27  
28  
29  
30  
31  
32  
33  
34  
35  
36  
37  
38  
39  
40  
41  
42  
43  
44  
45  
46  
47  
48  
49  
50  
51  
52  
53  
54  
55  
56  
57  
58  
59  
60

*5-methyl-4-oxo-N-(p-tolyl)-3,4-dihydrothieno[2,3-d]pyrimidine-6-carboxamide (23)* was prepared according to general procedure B using *p*-toluidine (80 mg, 0.75 mmol). Purification by reverse phase chromatography using the formic acid MDAP (gradient B over 15 min) gave the title product as a white solid (39 mg, 45 %). <sup>1</sup>H NMR (400 MHz, DMSO-d<sub>6</sub>) δ 12.54 (br. s, 1H), 10.10 (s, 1H), 8.17 (s, 1H), 7.56 (d, *J* = 8.5 Hz, 2H), 7.16 (d, *J* = 8.5 Hz, 2H), 2.72 (s, 3H), 2.28 (s, 3H); <sup>13</sup>C NMR (101 MHz, DMSO-d<sub>6</sub>) δ 164.1 (C), 160.4 (C=O), 158.3 (C=O), 147.3 (Ar-CH), 136.2 (C), 136.0 (C), 133.1 (C), 129.0 (2C, Ar-CH), 128.0 (C), 123.4 (C), 120.3 (2C, Ar-CH), 20.5 (CH<sub>3</sub>), 15.0 (CH<sub>3</sub>); LCMS (ESI, formic) *m/z* 300.11 [M+H]<sup>+</sup>, *R*<sub>t</sub> = 0.85 min; HRMS (ESI) calcd for C<sub>15</sub>H<sub>13</sub>N<sub>3</sub>O<sub>2</sub>S+H<sup>+</sup> 300.0801, found 300.0803 (4.19 min).

*5-methyl-4-oxo-N-(pyridin-3-yl)-3,4-dihydrothieno[2,3-d]pyrimidine-6-carboxamide (24)* was prepared according to general procedure B using pyridin-3-amine (57 mg, 0.61 mmol). Purification by reverse phase chromatography (5-20% acetonitrile (B) / 10 mM aqueous ammonium bicarbonate solution (A)). The product was dissolved in MeOH and transferred in a vial for test to give the title product as MeOH solvate, yellow solid (70 mg, 46 %). <sup>1</sup>H NMR (400 MHz, DMSO-d<sub>6</sub>) δ 12.59 (br. s, 1H), 10.39 (s, 1H), 8.84 (d, *J* = 2.5 Hz, 1H), 8.33 (dd, *J* = 5.0, 1.5 Hz, 1H), 8.19 (s, 1H), 8.07 - 8.14 (m, 1H), 7.40 (dd, *J* = 8.5, 5.0 Hz, 1H), 4.06 (d, *J* = 5.0 Hz, 1H, CH<sub>3</sub>OH), 3.17 (d, *J* = 5.0 Hz, 3H, CH<sub>3</sub>OH), 2.76 (s, 3H); LCMS (ESI, high pH) *m/z* 286.99 [M+H]<sup>+</sup>, *R*<sub>t</sub> = 0.52 min.

*N-(isoxazol-3-yl)-5-methyl-4-oxo-3,4-dihydrothieno[2,3-d]pyrimidine-6-carboxamide (25)*

A solution of 5-methyl-4-oxo-3,4-dihydrothieno[2,3-d]pyrimidine-6-carboxylic acid **16** (100 mg, 0.48 mmol) in thionyl chloride (2 mL, 27 mmol) was heated at 80 °C for 3 days before the reaction mixture was concentrated to dryness under reduced pressure. A solution of isoxazol-3-

1  
2  
3 amine (160 mg, 1.9 mmol) and DIPEA (0.2 mL, 1.2 mmol) in DMF (1.5 mL) dried over  
4  
5 molecular sieves (4 Å) was added to the crude and the reaction mixture was stirred at room  
6  
7 temperature with molecular sieves for 24 h. The crude reaction mixture was purified by reverse  
8  
9 phase chromatography using formic acid MDAP (gradient A over 15 min) to give the title  
10  
11 product as white solid (18 mg, 14 %). <sup>1</sup>H NMR (400 MHz, DMSO-d<sub>6</sub>) δ 11.98 (br. s, 2H), 8.85  
12  
13 (d, *J* = 1.5 Hz, 1H), 8.19 (s, 1H), 6.97 (d, *J* = 2.0 Hz, 1H), 2.75 (s, 3H); LCMS (ESI, formic) *m/z*  
14  
15 277.06 [M+H]<sup>+</sup>, *R*<sub>t</sub> = 0.57 min.  
16  
17  
18  
19

20  
21 *5-methyl-4-oxo-N-(thiophen-2-yl)-3,4-dihydrothieno[2,3-d]pyrimidine-6-carboxamide (26)*  
22  
23 was prepared according to general procedure B using thiophen-2-amine (64 mg, 0.65 mmol) at  
24  
25 40 °C. Purification by reverse phase chromatography using the formic acid MDAP (gradient B  
26  
27 over 15 min) to give the title product as a brown solid (21 mg, 15 %). <sup>1</sup>H NMR (400 MHz,  
28  
29 DMSO-d<sub>6</sub>) δ 12.59 (br. s, 1H), 11.42 (s, 1H), 8.19 (d, *J* = 4.0 Hz, 1H), 7.05 (t, *J* = 4.0 Hz, 1H),  
30  
31 6.90 - 6.93 (m, 2H), 2.76 (s, 3H); <sup>13</sup>C NMR (101 MHz, DMSO-d<sub>6</sub>) δ 164.4 (C), 158.5 (C=O),  
32  
33 158.2 (C=O), 147.6 (Ar-CH), 139.2 (C), 138.0 (C), 125.4 (C), 124.1 (C), 123.5 (Ar-CH), 117.9  
34  
35 (Ar-CH), 112.8 (Ar-CH), 15.1 (CH<sub>3</sub>); LCMS (ESI, formic) *m/z* 292.03 [M+H]<sup>+</sup>, *R*<sub>t</sub> = 0.74 min;  
36  
37 HRMS (ESI) calcd for C<sub>12</sub>H<sub>9</sub>N<sub>3</sub>O<sub>2</sub>S<sub>2</sub>+H<sup>+</sup> 292.0214, found 292.0214 (4.01 min).  
38  
39  
40  
41  
42

43 *5-methyl-4-oxo-N-(1,3,4-thiadiazol-2-yl)-3,4-dihydrothieno[2,3-d]pyrimidine-6-carboxamide*  
44  
45 (27) was prepared according to general procedure B using 2-amino-1,3,4-thiadiazole (62 mg,  
46  
47 0.613 mmol) at 40 °C. DMSO (2 mL) was added to the reaction mixture and the whole  
48  
49 solubilised with heating. After cooling a solid precipitated out which was collected by filtration  
50  
51 and dried in a vacuum oven overnight to give the title product as yellow solid (70 mg, 50 %). <sup>1</sup>H  
52  
53 NMR (400 MHz, DMSO-d<sub>6</sub>) δ 14.10 (br. s, 1H), 12.54 (br. s, 1H), 9.04 (br. s, 1H), 8.18 (d, *J* =  
54  
55 3.5 Hz, 1H), 2.89 (s, 3H); <sup>13</sup>C NMR (126 MHz, DMSO-d<sub>6</sub>) δ 167.6 (C), 166.7 (C=O), 158.5  
56  
57  
58  
59  
60

(C=O), 146.2 (Ar-CH), 144.9 (Ar-CH), 135.6 (C), 134.2 (C), 124.2 (C), 109.5 (C), 14.8 (CH<sub>3</sub>); LCMS (ESI, formic)  $m/z$  294.03 [M+H]<sup>+</sup>,  $R_t$  = 0.38 min; HRMS (ESI) calcd for C<sub>10</sub>H<sub>7</sub>N<sub>5</sub>O<sub>2</sub>S<sub>2</sub>+H<sup>+</sup> 294.0119, found 294.0115 (3.22 min); IR (ATR) cm<sup>-1</sup> 3142, 3095, 3007, 2930, 1676, 1651, 1552.

*Ethyl 2-(2-(5-methyl-4-oxo-3,4-dihydrothieno[2,3-d]pyrimidine-6-carboxamido)phenyl)acetate (28)* was prepared according to general procedure B using ethyl 2-(2-aminophenyl)acetate **48** (66 mg, 0.4 mmol). The crude product was purified by reverse phase chromatography using formic acid MDAP (gradient B over 15 min) to give the title product as a yellow solid (46 mg, 40 %). <sup>1</sup>H NMR (400 MHz, DMSO-d<sub>6</sub>)  $\delta$  12.56 (br. s, 1H), 9.75 (s, 1H), 8.17 (d,  $J$  = 4.0 Hz, 1H), 7.42 (br. d,  $J$  = 8.0 Hz, 1H), 7.29 - 7.36 (m, 2H), 7.19 - 7.28 (m, 1H), 4.04 (q,  $J$  = 7.0 Hz, 2H), 3.73 (s, 2H), 2.76 (s, 3H), 1.13 (t,  $J$  = 7.0 Hz, 3H); LCMS (ESI, formic)  $m/z$  372.07 [M+H]<sup>+</sup>,  $R_t$  = 0.83 min.

*2-(2-(5-methyl-4-oxo-3,4-dihydrothieno[2,3-d]pyrimidine-6-carboxamido)phenyl)acetic acid (29)* A solution of ethyl 2-(2-(5-methyl-4-oxo-3,4-dihydrothieno[2,3-d]pyrimidine-6-carboxamido)phenyl)acetate **28** (30 mg, 0.1 mmol) and lithium hydroxide (5.8 mg, 0.2 mmol) in a mixture of THF (0.4 mL), MeOH (0.2 mL) and water (0.1 mL) was stirred at room temperature for 2 h. Solvents were removed under a stream of nitrogen. The resulting crude product was dissolved in water (0.5 mL) and 2 M aqueous HCl solution was added. The resulting precipitate was collected by filtration and dried in a vacuum oven overnight to give the title product as a brown solid (16 mg, 58 %). <sup>1</sup>H NMR (400 MHz, DMSO-d<sub>6</sub>)  $\delta$  12.55 (br. s, 1H), 12.41 (br. s, 1H), 9.74 (s, 1H), 8.17 (d,  $J$  = 3.5 Hz, 1H), 7.46 (br. d,  $J$  = 7.5 Hz, 1H), 7.28 - 7.36 (m, 2H), 7.18 - 7.25 (m, 1H), 3.66 (s, 2H), 2.77 (s, 3H); LCMS (ESI, formic)  $m/z$  344.09 [M+H]<sup>+</sup>,  $R_t$  = 0.64 min.

1  
2  
3 N-(2-(hydroxymethyl)phenyl)-5-methyl-4-oxo-3,4-dihydrothieno[2,3-d]pyrimidine-6-  
4  
5  
6 carboxamide (**30**) TBAF (1 M in THF, 0.39 mL, 0.39 mmol) was added to a solution of N-(2-  
7  
8  
9  
10  
11  
12  
13  
14  
15  
16  
17  
18  
19  
20  
21  
22  
23  
24  
25  
26  
27  
28  
29  
30  
31  
32  
33  
34  
35  
36  
37  
38  
39  
40  
41  
42  
43  
44  
45  
46  
47  
48  
49  
50  
51  
52  
53  
54  
55  
56  
57  
58  
59  
60

N-(2-(hydroxymethyl)phenyl)-5-methyl-4-oxo-3,4-dihydrothieno[2,3-d]pyrimidine-6-carboxamide (**30**) TBAF (1 M in THF, 0.39 mL, 0.39 mmol) was added to a solution of N-(2-(((*tert*-butyldimethylsilyl)oxy)methyl)phenyl)-5-methyl-4-oxo-3,4-dihydrothieno[2,3-d]pyrimidine-6-carboxamide **50** (83 mg, 0.2 mmol) in THF (1 mL). The reaction mixture was stirred at room temperature for 3 h. Saturated aqueous NaHCO<sub>3</sub> solution (10 mL) and EtOAc (10 mL) were added. The organic layer was separated and the aqueous was extracted with EtOAc (2 x 10 mL). The combined organic layers were passed through a hydrophobic frit and concentrated under reduced pressure. The crude product was purified by reverse phase chromatography using the formic acid MDAP (gradient C over 15 min) to give the title product as a white solid (36 mg, 59 %). <sup>1</sup>H NMR (400 MHz, DMSO-d<sub>6</sub>) δ 12.57 (br. s, 1H), 9.87 (br. s, 1H), 8.18 (s, 1H), 7.79 (br. d, *J* = 8.0 Hz, 1H), 7.40 (br. d, *J* = 7.5 Hz, 1H), 7.30 (br. t, *J* = 8.0 Hz, 1H), 7.19 (br. t, *J* = 7.5 Hz, 1H), 5.63 (br. s, 1H), 4.61 (s, 2H), 2.83 (s, 3H); LCMS (ESI, formic) *m/z* 316.00 [M+H]<sup>+</sup>, *R*<sub>t</sub> = 0.67 min; HRMS (ESI) calcd for C<sub>15</sub>H<sub>13</sub>N<sub>3</sub>O<sub>3</sub>S+H<sup>+</sup> 316.0741, found 316.0756 (3.68min).

5-methyl-4-oxo-N-(2-sulfamoylphenyl)-3,4-dihydrothieno[2,3-d]pyrimidine-6-carboxamide (**31**). A solution of 5-methyl-4-oxo-3,4-dihydrothieno[2,3-d]pyrimidine-6-carboxylic acid **16** (60 mg, 0.29 mmol) in thionyl chloride (2 mL, 27 mmol) was refluxed for 16 h before the reaction mixture was concentrated under reduced pressure. A solution of 2-aminobenzenesulfonamide (59.0 mg, 0.34 mmol) and DIPEA (0.1 mL, 0.6 mmol) in DMF (1.5 mL) was dried over molecular sieves (4 Å) and then added to the acid chloride intermediate under nitrogen. The reaction mixture was stirred at room temperature under nitrogen for 5 h. The crude product was purified by reverse phase chromatography using the formic acid MDAP (gradient A over 15 min) to give the title product as an orange solid (11 mg, 11 %). <sup>1</sup>H NMR (400 MHz, DMSO-d<sub>6</sub>) δ



1  
2  
3 12.56 (br. s, 1H), 8.17 (d,  $J = 3.5$  Hz, 1H), 7.67 (dd,  $J = 8.0, 1.5$  Hz, 1H), 7.29 - 7.36 (m, 1H),  
4  
5 6.84 (d,  $J = 8.5$  Hz, 1H), 6.68 - 6.74 (m, 1H), 2.69 (s, 3H), amide NH and NH<sub>2</sub> protons not  
6  
7 visible; LCMS (ESI, formic)  $m/z$  364.97 [M+H]<sup>+</sup>,  $R_t = 0.62$  min.  
8  
9

10  
11 *5-methyl-N-(2-(methylsulfonyl)phenyl)-4-oxo-3,4-dihydrothieno[2,3-d]pyrimidine-6-*  
12 *carboxamide (32)*. 5-methyl-4-oxo-3,4-dihydrothieno[2,3-d]pyrimidine-6-carboxylic acid **16**  
13  
14 (100 mg, 0.48 mmol) in thionyl chloride (2 mL, 27 mmol) was heated at 50 °C for 2 days before  
15  
16 the reaction mixture was concentrated under reduced pressure. A solution of DMF (1.5 mL) and  
17  
18 DIPEA (0.2 mL, 1.1 mmol) dried over molecular sieves (4 Å) was added to the crude  
19  
20 intermediate followed by 2-(methylsulfonyl)aniline (250 mg, 1.5 mmol). The reaction mixture  
21  
22 was stirred at room temperature with molecular sieves under nitrogen for 16 h before being  
23  
24 heated to 50 °C for a further 16 h. The crude mixture was purified by reverse phase  
25  
26 chromatography using the formic acid MDAP (gradient B over 15 min) to give the title product  
27  
28 as a yellow solid (16 mg, 9%). <sup>1</sup>H NMR (400 MHz, DMSO-d<sub>6</sub>)  $\delta$  8.19 - 8.24 (m, 2H), 7.96 (dd,  
29  
30  $J = 8.0, 1.5$  Hz, 1H), 7.75 - 7.81 (m, 1H), 7.47 (td,  $J = 8.5, 1.0$  Hz, 1H), 3.33 (s, 3H), 2.85 (s,  
31  
32 3H), amide NH protons not visible; LCMS (ESI, formic)  $m/z$  364.11 [M+H]<sup>+</sup>,  $R_t = 0.76$  min.  
33  
34  
35  
36  
37  
38  
39

40  
41 *N-(4-carbamoylphenyl)-3,4-dichlorobenzamide (36)*. HATU (191 mg, 0.5 mmol), 4-  
42  
43 aminobenzamide (68 mg, 0.5 mmol) and DIPEA (0.15 mL, 0.84 mmol) were added to a solution  
44  
45 of 3,4-dichlorobenzoic acid (80 mg, 0.42 mmol) in DMF (1.5 mL) and the reaction mixture was  
46  
47 stirred at room temperature for 3 h. Saturated aqueous sodium bicarbonate solution (25 mL) was  
48  
49 added and the aqueous phase was extracted with DCM (2 x 25 mL). Solid was present in both  
50  
51 phases. The solid was collected by filtration under vacuum and dried in a vacuum oven to give  
52  
53 the title product as a white solid (87 mg, 65%). <sup>1</sup>H NMR (400 MHz, DMSO-d<sub>6</sub>)  $\delta$  10.55 (br. s,  
54  
55  
56  
57  
58  
59  
60

1  
2  
3 1H), 8.23 (d,  $J = 2.0$  Hz, 1H), 7.95 (dd,  $J = 8.5, 2.0$  Hz, 1H), 7.77 - 7.91 (m, 6H), 7.24 (br. s,  
4  
5 1H); LCMS (ESI, formic)  $m/z$  309.03  $[M+H]^+$ ,  $R_t = 0.92$  min.  
6  
7

### 8 9 **General Procedure C for Suzuki Coupling**

10  
11  
12 A mixture of the appropriate aryl halide (1 eq.), (1*H*-pyrazol-3-yl)boronic acid.3H<sub>2</sub>O (2 eq.),  
13 Pd(PPh<sub>3</sub>)<sub>4</sub> (15 mol%), NMP and saturated aqueous sodium carbonate solution (1 eq.) was heated  
14  
15 at 130 °C for 20 min in a microwave reactor. The reaction mixture was filtered and solvent was  
16  
17 evaporated. The crude product was purified by reverse phase chromatography to give the desired  
18  
19 final product  
20  
21  
22

23  
24  
25 N-(4-(1*H*-pyrazol-3-yl)phenyl)benzamide (**37**) was prepared according to general procedure C  
26  
27 using N-(4-bromophenyl)benzamide **43** (55 mg, 0.2 mmol). The crude product was purified by  
28  
29 reverse phase chromatography using the formic acid MDAP (gradient B over 15 min) to give the  
30  
31 title product as a white solid (35 mg, 67 %). <sup>1</sup>H NMR (400 MHz, DMSO-d<sub>6</sub>)  $\delta$  13.20-12.80 (2 br.  
32  
33 s, 1H, two pyrazole isomers visible), 10.27 (br. s, 1H), 7.93 - 8.01 (m, 2H), 7.70 - 7.88 (m, 5H),  
34  
35 7.48 - 7.64 (m, 3H), 6.68 (br. s, 1H); LCMS (ESI, formic)  $m/z$  264.11  $[M+H]^+$ ,  $R_t = 0.82$  min;  
36  
37 HRMS (ESI) calcd for C<sub>16</sub>H<sub>13</sub>N<sub>3</sub>O+H<sup>+</sup> 264.1131, found 264.1125 (3.99 min).  
38  
39  
40  
41  
42

43  
44 2-(2-((4-(1*H*-pyrazol-3-yl)phenyl)carbamoyl)phenyl)acetic acid (**38**) was prepared according  
45  
46 to general procedure C using methyl 2-(2-((4-bromophenyl)carbamoyl)phenyl)acetate **44** (60 mg,  
47  
48 0.172 mmol). The crude product was purified by reverse phase chromatography using the formic  
49  
50 acid MDAP (gradient B over 15 min) to give the title product as a white solid (33 mg, 60 %). <sup>1</sup>H  
51  
52 NMR (600 MHz, DMSO-d<sub>6</sub>)  $\delta$  12.59 (br. s, 1H), 10.47 (br. s, 1H), 7.73 - 7.79 (m, 5H), 7.68 (br.  
53  
54 s, 1H), 7.60 (d,  $J = 7.5$  Hz, 1H), 7.44 - 7.48 (m, 1H), 7.34 - 7.42 (m, 2H), 6.65 (d,  $J = 2.0$  Hz,  
55  
56  
57  
58  
59  
60

1  
2  
3 1H), 3.84 (s, 2H); LCMS (ESI, formic)  $m/z$  322.07  $[M+H]^+$ ,  $R_t$  = 0.72 min; HRMS (ESI) calcd  
4 for  $C_{18}H_{15}N_3O_3+H^+$  322.1186, found 322.1187 (3.64min).  
5  
6  
7

8  
9 *N*-(4-carbamoylphenyl)benzamide (**39**). HATU (300 mg, 0.8 mmol), 4-aminobenzamide (107  
10 mg, 0.8 mmol) and DIPEA (0.23 mL, 1.3 mmol) were added to a solution of benzoic acid (80  
11 mg, 0.66 mmol) in DMF (1.5 mL) and the reaction mixture was stirred at room temperature  
12 overnight. Saturated aqueous sodium bicarbonate solution (25 mL) was added and the aqueous  
13 phase was extracted with DCM (2 x 25 mL). Some solid remained in the aqueous phase and was  
14 collected by filtration. LCMS of the solid and the organic phase showed desired product present  
15 in both. The organic phase was passed through a hydrophobic frit and concentrated under  
16 reduced pressure. The resulting crude product was combined with the solid isolated by filtration  
17 prior purification. The resulting crude was purified by reverse phase chromatography using the  
18 formic acid MDAP (gradient B over 15 min) to give the title product as a white solid (67 mg, 41  
19 %).  $^1H$  NMR (400 MHz, DMSO- $d_6$ )  $\delta$  10.41 (s, 1H), 7.92 - 8.02 (m, 2H), 7.78 - 7.92 (m, 5H),  
20 7.57 - 7.66 (m, 1H), 7.49 - 7.58 (m, 2H), 7.22 (br. s, 1H);  $^{13}C$  NMR (101 MHz, DMSO- $d_6$ )  $\delta$   
21 167.3 (C=O), 165.8 (C=O), 141.8 (C), 134.7 (C), 131.7 (2C, Ar-CH), 129.1 (2C, Ar-CH), 128.4  
22 (2C, Ar-CH), 128.2 (2C, Ar-CH), 127.7 (C), 119.3 (Ar-CH); LCMS (ESI, formic)  $m/z$  241.11  
23  $[M+H]^+$ ,  $R_t$  = 0.66 min; HRMS (ESI) calcd for  $C_{14}H_{12}N_2O_2+H^+$  241.0972, found 241.0967 (3.29  
24 min); IR (ATR)  $cm^{-1}$  3383, 3308, 3163, 1650, 1606, 1516.  
25  
26  
27  
28  
29  
30  
31  
32  
33  
34  
35  
36  
37  
38  
39  
40  
41  
42  
43  
44  
45  
46  
47

48 *4*-(1-oxo-3,4-dihydroisoquinolin-2(1H)-yl)benzamide (**40**). A mixture of 4-(1-oxo-3,4-  
49 dihydroisoquinolin-2(1H)-yl)benzamide (**46**) (40 mg, 0.16 mmol), 2 M aqueous NaOH solution  
50 (1.2 mL, 2.4 mmol) and 30 % aqueous  $H_2O_2$  solution (54  $\mu$ L, 0.53 mmol) in EtOH (1 mL) was  
51 heated at 50  $^{\circ}C$  for 20 h. The reaction mixture was poured in saturated aqueous sodium sulfite  
52 solution and acidified to pH 1 with aqueous  $H_2SO_4$  solution. The mixture was concentrated under  
53  
54  
55  
56  
57  
58  
59  
60

1  
2  
3 reduced pressure. Water and DCM were added. The aqueous phase was extracted with DCM.  
4  
5 The combined organic phases were passed through a hydrophobic frit and concentrated under  
6  
7 reduced pressure. The resulting crude product was purified by reverse phase chromatography  
8  
9 using the formic acid MDAP (gradient B over 15 min) to give the title product as a white solid (8  
10  
11 mg, 19 %);  $^1\text{H}$  NMR (400 MHz,  $\text{DMSO-d}_6$ )  $\delta$  7.86 - 8.00 (m, 4H), 7.45 - 7.58 (m, 3H), 7.35 -  
12  
13 7.44 (m, 2H), 7.27 - 7.34 (m, 1H), 4.00 (t,  $J = 6.5$  Hz, 2H), 3.14 (t,  $J = 6.5$  Hz, 2H); LCMS (ESI,  
14  
15 formic)  $m/z$  267.07  $[\text{M}+\text{H}]^+$ ,  $R_t = 0.71$  min; HRMS (ESI) calcd for  $\text{C}_{16}\text{H}_{15}\text{N}_2\text{O}_2+\text{H}^+$  267.1128,  
16  
17 found 267.1125 (3.56 min).  
18  
19  
20  
21  
22

23  
24 *N*-(2-(1*H*-pyrazol-3-yl)pyrimidin-5-yl)benzamide (**41**) was prepared according to general  
25  
26 procedure C using *N*-(2-chloropyrimidin-5-yl)benzamide **45** (60 mg, 0.26 mmol). The resulting  
27  
28 crude product was purified by reverse phase chromatography using the high pH MDAP (gradient  
29  
30 B over 15 min) to give the title product as a white solid (28 mg, 41 %).  $^1\text{H}$  NMR (400 MHz,  
31  
32  $\text{DMSO-d}_6$ )  $\delta$  13.02 - 13.79 (br. d, 1H, two pyrazole isomers visible), 10.68 (br. s, 1H), 9.23 (s,  
33  
34 2H), 8.00 - 8.05 (m, 2H), 7.62 - 7.68 (m, 2H), 7.55 - 7.61 (m, 2H), 6.90 (d,  $J = 1.5$  Hz, 1H);  $^{13}\text{C}$   
35  
36 NMR (101 MHz,  $\text{DMSO-d}_6$ )  $\delta$  177.6 (Ar-CH), 165.9 (C=O), 148.5 (2C, Ar-CH), 133.7 (C),  
37  
38 132.6 (C), 132.2 (Ar-CH), 128.5 (2C, Ar-CH), 127.7 (2C, Ar-CH), 119.1 (C), 105.4 (Ar-CH),  
39  
40 one carbon too weak to assign should be around 150 ppm; LCMS (ESI, high pH)  $m/z$  266.04  
41  
42  $[\text{M}+\text{H}]^+$ ,  $R_t = 0.74$  min; HRMS (ESI) calcd for  $\text{C}_{14}\text{H}_{11}\text{N}_5\text{O}+\text{H}^+$  266.1029, found 266.1036  
43  
44 (3.47min).  
45  
46  
47  
48  
49

50  
51 *2*-(4-(1*H*-pyrazol-3-yl)phenyl)-3,4-dihydroisoquinolin-1(2*H*)-one (**42**) was prepared according  
52  
53 to general procedure C using 2-(4-bromophenyl)-3,4-dihydroisoquinolin-1(2*H*)-one **47** (100 mg,  
54  
55 0.331 mmol). The resulting crude product was purified by reverse phase chromatography using  
56  
57 the formic acid MDAP (15-55%(B) over 15 mins) to give the title product as a white solid (45  
58  
59  
60

1  
2  
3 mg, 47 %).  $^1\text{H}$  NMR (400 MHz, DMSO- $d_6$ )  $\delta$  13.31 + 12.89 (2 br. s, 1H), 7.95 (dd,  $J = 7.5$ , 1.0  
4 Hz, 1H), 7.75 - 7.88 (m, 3H), 7.54 (td,  $J = 7.5$ , 1.5 Hz, 1H), 7.46 (br. s, 1H), 7.36-7.43 (m, 3H),  
5  
6  
7 6.73 (br. s, 1H), 3.99 (t,  $J = 6.5$  Hz, 2H), 3.15 (t,  $J = 6.5$  Hz, 2H); LCMS (ESI, high pH)  $m/z$   
8  
9 290.23  $[\text{M}+\text{H}]^+$ ,  $R_t = 0.89$  min.

10  
11  
12  
13  
14 *N*-(4-bromophenyl)benzamide (**43**). HATU (335 mg, 0.88 mmol) and DIPEA (0.26 mL, 1.5  
15 mmol) were added to a solution of benzoic acid (90 mg, 0.74 mmol) in DMF (3 mL). The  
16  
17 mixture was stirred at room temperature for 5 min. 4-bromoaniline (152 mg, 0.88 mmol) was  
18  
19 then added and the reaction mixture was stirred at room temperature for 15 h. The crude reaction  
20  
21 mixture was purified by reverse phase chromatography (30-85 %  $\text{CH}_3\text{CN}$  + 0.01 % formic acid  
22  
23 (B) /  $\text{H}_2\text{O}$  + 0.01 % formic acid (A), 43 g C18 column) to give the title product as a white solid  
24  
25 (120 mg, 49 %).  $^1\text{H}$  NMR (400 MHz, DMSO- $d_6$ )  $\delta$  10.34 (s, 1H), 7.94 (br. d,  $J = 7.0$  Hz, 2H),  
26  
27 7.77 (br. d,  $J = 9.0$  Hz, 2H), 7.59-7.62 (m, 1H), 7.50 - 7.56 (m, 4H); LCMS (ESI, formic)  $m/z$   
28  
29 275.97 + 277.93  $[\text{M}+\text{H}]^+$ ,  $R_t = 1.09$  min.

30  
31  
32  
33  
34  
35  
36 *Methyl 2*-(2-((4-bromophenyl)carbamoyl)phenyl)acetate (**44**). HATU (335 mg, 0.88 mmol)  
37  
38 and DIPEA (0.26 mL, 1.49 mmol) were added to a solution of 2-(2-methoxy-2-oxoethyl)benzoic  
39  
40 acid (135 mg, 0.69 mmol) in DMF (3 mL). The mixture was stirred at room temperature for 5  
41  
42 min. 4-bromoaniline (152 mg, 0.88 mmol) was then added and the reaction mixture was stirred at  
43  
44 room temperature for 15 h. The crude reaction mixture was purified by reverse phase  
45  
46 chromatography (30-85 %  $\text{CH}_3\text{CN}$  + 0.01 % formic acid (B) /  $\text{H}_2\text{O}$  + 0.01 % formic acid (A), 43  
47  
48 g C18 column) to give the title product as a beige solid (210 mg, 68 %).  $^1\text{H}$  NMR (400 MHz,  
49  
50 DMSO- $d_6$ )  $\delta$  10.44 (s, 1H), 7.69 (br. d.,  $J = 9.0$  Hz, 2H), 7.60 (br. d,  $J = 7.5$  Hz, 1H), 7.34 - 7.54  
51  
52 (m, 5H), 3.90 (s, 2H), 3.53 (s, 3H); LCMS (ESI, formic)  $m/z$  347.97, 349.93  $[\text{M}+\text{H}]^+$ ,  $R_t = 1.08$   
53  
54  
55 min.  
56  
57  
58  
59  
60

1  
2  
3  
4 N-(2-chloropyrimidin-5-yl)benzamide (**45**). HATU (747 mg, 1.96 mmol) and DIPEA (0.57  
5 mL, 3.27 mmol) were added to a solution of benzoic acid (200 mg, 1.64 mmol) in DMF. The  
6  
7  
8 mixture was stirred at room temperature for 5 min. 2-Chloropyrimidin-5-amine (255 mg, 1.97  
9  
10 mmol) was then added and the reaction mixture was stirred at room temperature for 3 h. The  
11  
12 reaction mixture was then heated at 40 °C for 15 h. Additional 2-chloropyrimidin-5-amine (125  
13  
14 mg, 0.97 mmol) was added and the reaction mixture was heated at 40 °C for 5 h. Solvent was  
15  
16 evaporated under reduced pressure. The resulting crude product was purified by reverse phase  
17  
18 chromatography (20-60 % MeOH (B) / water + 0.1 % formic acid (A), C18 GOLD column) to  
19  
20 give the title product as a brown solid (175 mg, 46 %). <sup>1</sup>H NMR (400 MHz, DMSO-d<sub>6</sub>) δ 10.77  
21  
22 (br. s, 1H), 9.14 (s, 2H), 7.98 - 8.02 (m, 2H), 7.62 - 7.69 (m, 1H), 7.58 (apparent triplet, *J* = 7.0,  
23  
24 8.0 Hz, 2H); LCMS (ESI, high pH) *m/z* 234.09 [M+H]<sup>+</sup>, *R*<sub>t</sub> = 0.84 min.  
25  
26  
27  
28  
29

30  
31 4-(1-oxo-3,4-dihydroisoquinolin-2(1H)-yl)benzotrile (**46**). A mixture of 3,4-  
32  
33 dihydroisoquinolin-1(2H)-one (62 mg, 0.42 mmol), 4-iodobenzotrile (195 mg, 0.85 mmol),  
34  
35 potassium carbonate (59 mg, 0.43 mmol) and copper(I) iodide (16 mg, 0.084 mmol) in DMF (1  
36  
37 mL) was heated at 160 °C overnight under nitrogen. The reaction mixture was cooled and poured  
38  
39 into saturated aqueous NH<sub>4</sub>OH solution and EtOAc. The phases were separated and the aqueous  
40  
41 phase was extracted with EtOAc. The combined organic phases were washed with brine,  
42  
43 separated, passed through a hydrophobic frit and concentrated under reduced pressure. The  
44  
45 resulting crude product was then purified by reverse phase chromatography using the formic acid  
46  
47 MDAP (gradient C over 15 min) to give the title product as a white solid (69 mg, 66 %). <sup>1</sup>H  
48  
49 NMR (400 MHz, DMSO-d<sub>6</sub>) δ 7.93 - 7.99 (m, 1H), 7.88 (d, *J* = 9.0 Hz, 2H), 7.66 (d, *J* = 9.0 Hz,  
50  
51 2H), 7.56 (td, *J* = 7.5, 1.5 Hz, 1H), 7.36 - 7.44 (m, 2H), 4.03 (t, *J* = 6.5 Hz, 2H), 3.15 (t, *J* = 6.5  
52  
53 Hz, 2H); LCMS (ESI, formic) *m/z* 249.12 [M+H]<sup>+</sup>, *R*<sub>t</sub> = 0.94 min.  
54  
55  
56  
57  
58  
59  
60

1  
2  
3  
4  
5  
6  
7  
8  
9  
10  
11  
12  
13  
14  
15  
16  
17  
18  
19  
20  
21  
22  
23  
24  
25  
26  
27  
28  
29  
30  
31  
32  
33  
34  
35  
36  
37  
38  
39  
40  
41  
42  
43  
44  
45  
46  
47  
48  
49  
50  
51  
52  
53  
54  
55  
56  
57  
58  
59  
60

*2-(4-bromophenyl)-3,4-dihydroisoquinolin-1(2H)-one (47)*. A mixture of 3,4-dihydroisoquinolin-1(2H)-one (200 mg, 1.36 mmol), 1-bromo-4-iodobenzene (769 mg, 2.72 mmol), copper(I) iodide (52 mg, 0.27 mmol) and potassium carbonate (207 mg, 1.495 mmol) in DMF (3 mL) was heated at 160 °C overnight. The reaction mixture was cooled and poured into saturated aqueous NH<sub>4</sub>OH solution and EtOAc. The two phases were separated and the aqueous phase was extracted with EtOAc. The combined organic phases were washed with brine, separated, passed through a hydrophobic frit and evaporated under reduced pressure. The resulting crude product was purified by reverse phase chromatography (Redisep C18 column GOLD, 50 g - 40-85 % acetonitrile (B)/ water + 0.1 % formic acid (A) gradient) to give the title product as a white solid (242 mg, 59 %). <sup>1</sup>H NMR (400 MHz, DMSO-d<sub>6</sub>) δ 7.94 (d, *J* = 8.0 Hz, 1H), 7.58-7.63 (m, 2H), 7.54 (td, *J* = 7.5, 1.5 Hz, 1H), 7.34-7.42 (m, 4H), 3.95 (t, *J* = 6.5 Hz, 2H), 3.13 (t, *J* = 6.5 Hz, 2H); LCMS (ESI, high pH) *m/z* 301.77 + 303.75 [M+H]<sup>+</sup>, *R*<sub>t</sub> = 1.09 min.

*Ethyl 2-(2-aminophenyl)acetate (48)*. A solution of ethyl 2-(2-nitrophenyl)acetate (200 mg, 0.96 mmol) in EtOH (40 mL) was pumped through an H-cube (10 % Pd/C catcart cartridge, 20 °C, full H<sub>2</sub>). Solvent was evaporated under reduced pressure to give the title product as an orange gum (148 mg, 86 %). <sup>1</sup>H NMR (400 MHz, DMSO-d<sub>6</sub>) δ 6.90 - 6.99 (m, 2H), 6.65 (dd, *J* = 8.0, 1.0 Hz, 1H), 6.51 (apparent dt, *J* = 7.5, 1.5 Hz, 1H), 4.84 (br. s, 2H), 4.07 (q, *J* = 7.0 Hz, 2H), 3.49 (s, 2H), 1.18 (t, *J* = 7.0 Hz, 3H); LCMS (ESI, formic) *m/z* 180.06 [M+H]<sup>+</sup>, *R*<sub>t</sub> = 0.70 min.

*2-(((tert-butyldimethylsilyl)oxy)methyl)aniline (49)*. *Tert*-butyldimethylsilyl chloride (673 mg, 4.47 mmol) and imidazole (553 mg, 8.12 mmol) were added to a solution of (2-aminophenyl)methanol (500 mg, 4.06 mmol) in CH<sub>2</sub>Cl<sub>2</sub> (6 mL). The reaction mixture was stirred at room temperature for 14 h. CH<sub>2</sub>Cl<sub>2</sub> (5 mL) and water (10 mL) were added and the organic layer was separated using a hydrophobic frit before being concentrated under reduced pressure to

1  
2  
3 give the title product as an orange liquid (889 mg, 92 %). <sup>1</sup>H NMR (400 MHz, DMSO-d<sub>6</sub>) δ 7.07  
4 (br. d, *J* = 7.5 Hz, 1H), 6.96 (apparent dt, *J* = 7.5, 1.5 Hz, 1H), 6.62 (dd, *J* = 8.0, 1.0 Hz, 1H),  
5  
6 6.54 (apparent dt, *J* = 7.5, 1.0 Hz, 1H), 4.83 (br. s., 2 H), 4.57 (s, 2H), 0.89 (s, 9H), 0.06 (s, 6H);  
7  
8 LCMS (ESI, formic) *m/z* 238.14 [M+H]<sup>+</sup>, R<sub>t</sub> = 1.36 min.  
9  
10  
11

12  
13 N-(2-(((*tert*-butyldimethylsilyl)oxy)methyl)phenyl)-5-methyl-4-oxo-3,4-dihydrothieno[2,3-  
14  
15 d]pyrimidine-6-carboxamide (**50**) was prepared according to general procedure B using 2-(((*tert*-  
16  
17 butyldimethylsilyl)oxy)methyl)aniline **49** (140 mg, 0.59 mmol). The crude product was purified  
18  
19 by reverse phase chromatography (43 g C18 column, 40-80 % CH<sub>3</sub>CN + 0.1% formic acid (B) /  
20  
21 H<sub>2</sub>O + 0.1% formic acid (A) over 25 min) to give the title product as a yellow solid (90 mg, 44  
22  
23 %). <sup>1</sup>H NMR (400 MHz, DMSO-d<sub>6</sub>) δ 12.57 (br. s, 1H), 9.63 (s, 1H), 8.18 (s, 1H), 7.60 (dd, *J* =  
24  
25 8.0, 1.0 Hz, 1H), 7.46 (dd, *J* = 7.5, 1.0 Hz, 1H), 7.32 (apparent td, *J* = 8.0, 1.5 Hz, 1H), 7.26  
26  
27 (apparent td, *J* = 7.5, 1.0 Hz, 1H), 4.77 (s, 2H), 2.80 (s, 3H), 0.87 (s, 9H), 0.06 (s, 6H). LCMS  
28  
29 (ESI, formic) *m/z* 430.14 [M+H]<sup>+</sup>, R<sub>t</sub> = 1.32 min.  
30  
31  
32  
33  
34  
35

### 36 Chemi-Luminescent Nitrogen Detection (CLND) solubility determination

37  
38  
39 GSK in-house kinetic solubility assay: 5 μL of 10 mM DMSO stock solution was diluted to  
40  
41 100 μL with pH 7.4 phosphate buffered saline, equilibrated for 1 hour at room temperature and  
42  
43 filtered through Millipore Multiscreen<sub>HTS</sub>-PCF filter plates (MSSL BPC). The filtrate was  
44  
45 quantified by suitably calibrated flow injection Chemi-Luminescent Nitrogen Detection. The  
46  
47 standard error of the CLND solubility determination is ±30 μM, the upper limit of the solubility  
48  
49 was 500 μM when working from 10 mM DMSO stock solution.  
50  
51  
52  
53  
54

### 55 Calculated Properties



1  
2  
3 Calculated partition coefficient (clogP) was computed using the BioByte algorithm, version  
4  
5 5.4 (BioByte Corp., 201 W. 4th St., #204, Claremont, CA 91711-4707)  
6  
7

### 8 9 **BCATm fluorescent assay**

10  
11 All reagents were purchased from Sigma-Aldrich Ltd. (Gillingham, Dorset, UK) unless  
12 otherwise stated. Assay buffer was 50 mM HEPES (pH 7.5), 50 mM NaCl and 1 mM CHAPS.  
13  
14 Horseradish Peroxidase was initially diluted to 500 units/ml in water. 4-methyl-2-oxovalerate  
15  
16 was initially diluted to 10 mM in assay buffer. L-Leucine and  $\alpha$ -ketoglutarate were both initially  
17  
18 diluted to 100 mM in 50 mM HEPES (pH 7.5) with pyridoxal phosphate (PLP) initially diluted  
19  
20 to 10 mM in 50 mM HEPES (pH 7.5). Amplex red (Invitrogen, Paisley, UK) was initially diluted  
21  
22 to 20 mM in DMSO.  
23  
24  
25  
26  
27  
28

29  
30 BCATm and L-GOX protein were cloned, expressed, and isolated in house (GSK, Stevenage,  
31  
32 UK). The assay monitors the production of L-glutamate from branch chain amino-acids and  $\alpha$ -  
33  
34 ketoglutarate through the coupling of hBCATm activity to two additional enzymes, L-Glutamate  
35  
36 Oxidase (L-GOx) and Horseradish Peroxidase (HRP). L-GOx catabolises L-glutamate to  
37  
38 generate  $\alpha$ -Ketoglutarate and hydrogen peroxide, the latter being utilised by HRP and leading to  
39  
40 the formation of fluorescent resorufin from the redox sensitive dye Amplex Red.  
41  
42  
43  
44

45  
46 The BCATm fluorescent assay was carried out in low volume 384-well plates (Greiner Bio-  
47  
48 one, Stonehouse, UK) at a final volume of 10  $\mu$ L per well. Test compounds were added to plates  
49  
50 as 50 nL solutions in DMSO using an Echo 555 acoustic dispenser (Labcyte, Sunnyvale, CA)  
51  
52 prior to the addition of assay components. Additionally, 50 nL DMSO or positive control (5-  
53  
54 chloro-2benzenzofurancarboxylic acid 2-[[2-(trifluoromethyl)phenyl]sulfonyl] hydrazide;  
55  
56 emolecules) was included in two columns each to give 100% activity and 100% inhibition  
57  
58  
59  
60

1  
2  
3 controls, respectively. Single-concentration testing was at 10  $\mu\text{M}$  compound concentration. For  
4  
5  $\text{pIC}_{50}$  determination, compounds were tested using an 11-point, three-fold dilution series from  
6  
7  
8 either 625  $\mu\text{M}$  or 6.25  $\mu\text{M}$  prepared using a Biomek FX (Beckman Coulter, Wycombe, UK).  
9

10  
11 To these compound plates, 4  $\mu\text{L}$  of an enzyme-PLP solution containing 20 nM BCATm and 40  
12  
13 nM PLP in assay buffer was added. Following this, 4  $\mu\text{L}$  of a coupling solution containing 3 mM  
14  
15 L-Leucine, 0.5 mM  $\alpha$ -ketoglutarate, 10 units/mL HRP and 80  $\mu\text{M}$  Amplex red in assay buffer  
16  
17 was added to initiate the reaction. The coupling solution was incubated on a roller at room  
18  
19 temperature in a 15 mL tube with 1 mL Agarose immobilised Catalase (Sigma-Aldrich Ltd.) per  
20  
21 10 mL of coupling solution to 'scrub' the coupling solution prior to addition of Amplex Red and  
22  
23 remove background levels of hydrogen peroxide. After a 10 minute incubation, 2  $\mu\text{L}$  of 100 mM  
24  
25 4-methyl-2-oxovalerate was added to stop the reaction.  
26  
27  
28  
29  
30

31 Final assay concentrations were 10 nM BCATm, 20 nM PLP, 5 units per mL HRP, 1.5 mM L-  
32  
33 Leucine, 0.25 mM alpha-ketoglutarate and 40  $\mu\text{M}$  Amplex Red. All additions were performed  
34  
35 using a Multidrop Combi (Thermo Fisher Scientific, Waltham, MA). Plates were transferred to  
36  
37 an EnVision reader (PerkinElmer) (excitation filter 525/20 nm; emission filter 598/25 nm).  
38  
39  
40  
41  
42  
43  
44

#### 45 **BCAT cellular assay**

46  
47  
48 Differentiated primary human adipocytes (Zenbio) were challenged overnight using  
49  
50 compounds dissolved in HBSS (Gibco 1g/L glucose) complemented with HEPES 10 mM, L-  
51  
52 Serine 50  $\mu\text{M}$  and L-Leucine 150  $\mu\text{M}$ . Next day cell supernatant were subjected to amino acids  
53  
54 determinations using HPLC analysis essentially as previously described.<sup>4</sup> The method is based  
55  
56  
57  
58  
59  
60

1  
2  
3 on automated, online derivatization using o-phthalaldehyde (OPA) for primary amino acids and  
4  
5 9-fluorenylmethyl chloroformate (FMOC) for secondary amino acids, using an Eclipse Plus C18  
6  
7 3x10mm 3.5 $\mu$ m column to perform reversed phase HPLC (all chemicals and hardware from  
8  
9 Agilent Technologies, Inc.). The percentage of inhibition was calculated on leucine  
10  
11 concentration remaining compared to vehicle treated cells.  
12  
13

### 14 15 16 **Analogue Searching**

17  
18  
19 FindAnalogues is an in-house developed PipelinePilot® [Pipeline Pilot (2010) Accelrys Ltd,  
20  
21 San Diego] protocol developed to search for analogues of fragment compounds. The protocol  
22  
23 used several search methods to retrieve analogues of fragment structures. The tautomers of the  
24  
25 input molecule were enumerated prior to searching and core generation using the relevant  
26  
27 PipelinePilot component. Tautomers were also enumerated for the core. A core was generated  
28  
29 for each input query molecule by iteratively removing terminal chain atoms, stopping at O,N,S.  
30  
31 An amide/sulfonamide/ester/acid was cleaved to leave either N or C=O/SO<sub>2</sub>. Additional rules  
32  
33 break N-linked piperidines to leave N. Terminal Nitrogens are set to [#7]. [nH] to n.  
34  
35  
36  
37  
38

39  
40 The core was used to conduct a substructure search on the relevant database. The JChem  
41  
42 Cartridge was used for enabling chemical structure search and management within Oracle,  
43  
44 JChem 5.3, ChemAxon (<http://www.chemaxon.com>).  
45  
46

47  
48 Similarity searches were performed on the database using the full query molecule and the  
49  
50 ChemAxon fingerprint. Several similarity search metrics<sup>22</sup> were used: Tversky searches<sup>23</sup> using  
51  
52 the input molecule as both the target and the query with  $\alpha = 0.9$ ,  $\beta = 0.1$ , cut-off = 0.8;  
53  
54 Tanimoto search with similarity cut-off of 0.8. Additionally a reduced graph<sup>24</sup> substructure  
55  
56 search was performed with the reduced graph derived from the full query structure. Optionally,  
57  
58  
59  
60

1  
2  
3 limits could be placed on the hit list according to the difference in heavy atom count or  
4  
5 molecular weight difference between the query and the hit molecule. This was particularly  
6  
7 significant for the substructure and Tversky searches to control the size of the hit molecules. The  
8  
9 total number of hits from any single query could also be specified, defined as MaxHits in the  
10  
11 following. For the SS and RG search, hits were ordered by molecular weight and the MaxHits  
12  
13 lowest molecular weight compounds were returned. For the Tversky and Tanimoto search, the  
14  
15 MaxHits most similar compounds were returned.  
16  
17  
18  
19

### 20 21 **NMR Saturation transfer difference (STD):** 22

23  
24 All NMR spectra were recorded in PBS buffer [pH7.2], 100% D<sub>2</sub>O, 300K and Bruker Avance  
25  
26 700 MHz spectrometer, equipped with a 5mm cryo-probe and sample changer (Bruker-BioSpin).  
27  
28 Sample volume was 180  $\mu$ L in a 3mm sample tube (Norrell). A set of reference <sup>1</sup>H NMR spectra  
29  
30 for individual fragments was recorded in the absence of protein.  
31  
32  
33

34  
35 Fragments were tested for binding to BCAT in pools of typically 5 compounds per sample at a  
36  
37 concentration of 1 mM each. The protein concentration was 10  $\mu$ M. Saturation of protein <sup>1</sup>H  
38  
39 resonances was achieved by continuous wave irradiation at 0.3 ppm for 2 s. A 30-ms spin-lock  
40  
41 period was employed before acquisition to allow the residual protein signal to decay. STD  
42  
43 spectra were processed and deconvoluted by comparison with the reference spectra of the  
44  
45 individual compounds using the TOPSPIN program (Bruker BioSpin). Only STD signals to the  
46  
47 left of the waterline (i.e. > 5.5ppm) were evaluated. The intensity of the largest resolved signal of  
48  
49 each compound was determined and compared to the maximum noise level of the spectrum in  
50  
51 the signal-free region between 11 and 12 ppm. STD signals with an intensity 4x above noise  
52  
53 level were classified as hits.  
54  
55  
56  
57  
58  
59  
60

## T<sub>m</sub> Methods

The protein was diluted to a final concentration 2.4  $\mu\text{M}$  in buffer (25 mM HEPES pH 7.5 containing 25 mM NaCl, 20 mM DTT, 20 mM EDTA, 2.5 % glycerol). The PLP (E) form of the enzyme was prepared by incubation with a 100-fold excess of  $\alpha$ -ketoglutarate for 1 minute at 20  $^{\circ}\text{C}$ . The PMP (F) form of the enzyme was prepared by incubation with a 100-fold excess of l-leucine for 1 minute at 20  $^{\circ}\text{C}$ . The isoforms of the enzyme were purified by centrifugal ultrafiltration at 15000  $\times g$  at 4  $^{\circ}\text{C}$  for 15 minutes using Vivaspin-6 10 kDa nominal molecular cut-off spin filters. The retentates were recovered and the volume adjusted to give a final protein concentration of 2.4  $\mu\text{M}$ . The purified enzymes were stored at 4  $^{\circ}\text{C}$  until used. Samples were prepared in 96-well plates. 0.5  $\mu\text{L}$  of buffer (control), DMSO or compound at 10 mM in DMSO were aliquoted into separate wells. To each well was added 50  $\mu\text{L}$  of the required form of the enzyme containing a 1:1000 dilution of Sypro Orange (Invitrogen). The plate was incubated for 1 min at room temperature and centrifuged for 1 minute at 1000  $\times g$ . 20  $\mu\text{L}$  aliquots from each well were transferred to wells in sequential rows of a white 96-well plate (Abgene 0.2 mL semi-skirted Thermo-Fast plate; AB-0900/w) and overlaid with 5  $\mu\text{L}$  silicon oil. Data were acquired on an Exicycler rt-pcr instrument (Bioneer Inc). Fluorescence intensity was recorded at 0.5  $^{\circ}\text{C}$  intervals over a temperature range of 4  $^{\circ}\text{C}$  to 94  $^{\circ}\text{C}$  at a heating rate of 1  $^{\circ}\text{C}/\text{min}$ . The raw fluorescent intensity signals were exported into Excel csv format. The raw data were normalised using the formula:  $(\text{cell value} - \text{MIN}(\text{column data range})) / (\text{MAX}(\text{column data range}) - \text{MIN}(\text{column data range}))$  Where “cell value” is the raw fluorescence reading at each temperature point.

The normalised fluorescence intensities versus temperature data were fitted to a standard denaturation isotherm in Grafit5 (Erithacus software).

### BCATm/PLP protein production and crystallisation

Human branched-chain amino acid aminotransferase mitochondrial (BCATm) (residues 28-392) deleted of the N-terminal mitochondria signal peptide (residues 1-27) was cloned into Kanamycin resistant pET28a via NdeI/XhoI restriction endonuclease sites with an N-terminal 6His-Thrombin cleavage site. This was used to transform *E.coli* BL21 Star (DE3) (Invitrogen) cells. The transformed cells were grown in turbo media supplemented with glucose and kanamycin, after induction with IPTG 1mM the temperature was reduced from 37 °C to 25 °C and the cells harvested 23 hours later. The human BCATm was purified using a modification of the method described by Conway and Huston<sup>25</sup>, frozen cell pellets were thawed in buffer (25 mM HEPES, pH 7.5, 500 mM NaCl, 4 M Urea, 1 mM DTT, 20 mM Imidazole, Protease Inhibitor Cocktail III (MERCK) containing 0.1 mM Pyridoxal phosphate, 0.2 mg/ml lysozyme and 10 U/ml Benzonase (MERCK) and mixed for 30 minutes at room temperature. The cell suspension was sonicated and the cell debris removed by centrifugation at 100,000 g for 90mins. The supernatant was loaded onto a 5 ml HisTrap HP column (GE Healthcare), washed with 10 bed volumes (Bv) of buffer before running a gradient to 0 M Urea in buffer over 10 Bv at 5 ml/min. The column was eluted using a series of Imidazole steps 25, 50, 100, 200 and 500 mM in buffer (10 Bv of each at 5 ml/min). The human BCATm containing fractions (100 mM & 200 mM Imidazole step) were pooled and concentrated using Amicon Ultra (Millipore) centrifugal ultrafilters with a 30 kDa (MWCO) and further purified using a Superdex200 column (GE Healthcare). Dimeric human BCATm was pooled and buffer exchanged into thrombin cleavage buffer (50 mM HEPES, pH 7.5, 150 mM NaCl, 2 mM CaCl) and incubated for 2 hours at room temp with 10 U/ml of Thrombin (LeeBio). After cleavage, DTT and (NH<sub>4</sub>)<sub>2</sub>SO<sub>4</sub> was added at 1 mM and 1.5 M, respectively and the thrombin removed by purification on a Butyl Sepharose HP

1  
2  
3 column (GE Healthcare). Human BCATm was eluted using a gradient to 0M (NH<sub>4</sub>)<sub>2</sub>SO<sub>4</sub> over 20  
4  
5 Bv. The human BCATm was pooled, buffer exchanged into storage buffer (25 mM HEPES pH  
6  
7 7.5, 25 mM NaCl, 20 mM DTT, 20 mM EDTA, 2.5 % glycerol), concentrated to ~10 mg/ml and  
8  
9 snap frozen at -80 °C. Functional competency was confirmed using the coupled biochemical  
10  
11 assay. Structural integrity was confirmed using differential scanning fluorimetry measurements  
12  
13 and protein crystallisation.  
14  
15

16  
17  
18 The purified protein in 25 mM HEPES pH 7.5, 25 mM NaCl, 20 mM DTT, 20 mM EDTA, 2.5  
19  
20 % glycerol and concentrated to at least 7.6 mg/mL was used for crystallography. Crystals of  
21  
22 BCATm were grown by hanging drop vapour diffusion at 20 °C with microseeding using MDL  
23  
24 Morpheus™ screen condition B2 supplemented with 10 mM DTT in a protein to microseed  
25  
26 solution of drop ratio of 1:1. The Hampton Research seed-bead method was used to generate  
27  
28 microseeds. The crystals had a yellow hue suggestive of bound PLP cofactor despite none being  
29  
30 added during purification or crystallization. The complex with compound 27 was produced from  
31  
32 a cocrystal grown under comparable conditions to the holoenzyme but in the presence of the  
33  
34 compound (at 25 mM).  
35  
36  
37  
38  
39

### 40 **X-ray Crystallography - crystal structures of BCATm/PLP complexed with inhibitors**

41  
42  
43  
44 Holocrystals were transferred to soaking buffer comprising MDL Morpheus™ screen  
45  
46 condition B2 supplemented with 10 mM or 20 mM DTT and the compound of interest (from a  
47  
48 stock solution dissolved in DMSO) at the soaking concentration given in the X-ray summary  
49  
50 table (in supplementary data). Crystals were harvested in a cryo-loop and plunge-frozen into  
51  
52 liquid nitrogen before loading in a puck for mounting with a sample collector. Data from single  
53  
54 crystals were collected at 100 K either at the Diamond Light Source (Harwell) or on an in-house  
55  
56  
57  
58  
59  
60

1  
2  
3 RIGAKU FR-E<sup>+</sup> SUPERBRIGHT/Saturn A200 detector/ACTOR robotic system. Data  
4  
5 processing was achieved using DENZO<sup>26</sup>, MOSFLM<sup>27</sup> or XDS<sup>28</sup> (within AUTOPROC<sup>29</sup>) and  
6  
7 scaled using either SCALEPACK<sup>26</sup> or SCALA<sup>30</sup> within the CCP4 programming suite<sup>25</sup>.  
8  
9 Structures were solved by Fourier synthesis using REFMAC<sup>32</sup> (*via* CCP4) starting from a  
10  
11 previously determined in house structure, model-building was performed using COOT<sup>33</sup> and  
12  
13 refined using REFMAC *via* CCP4. The statistics for the data collection and refined co-ordinates  
14  
15 are given in Supplementary information. The final crystal structures are deposited in the Protein  
16  
17 Data Bank under the accession codes 5I5S-Y and 5I60.  
18  
19  
20  
21  
22

23 **Supporting Information.** Statistics for data collection and refined co-ordinates for X-ray  
24  
25 crystallography are given in the supporting information. This material is available free of charge  
26  
27 via the Internet at <http://pubs.acs.org>.  
28  
29  
30

## 31 AUTHOR INFORMATION

### 32 33 34 **Corresponding Author**

35  
36  
37 \*Phone +44 (0)1438 763875. Email [jennifer.a.borthwick@gsk.com](mailto:jennifer.a.borthwick@gsk.com)  
38  
39

### 40 **Author Contributions**

41  
42  
43 The manuscript was written through contributions of all authors. All authors have given approval  
44  
45 to the final version of the manuscript.  
46  
47

## 48 49 ACKNOWLEDGMENT

50  
51 The authors thank Tony Dean, Laurie Gordon and Andrew Leach for review of the manuscript.  
52  
53

## 54 55 ABBREVIATIONS

56  
57  
58  
59  
60



1  
2  
3 BCAT, branched-chain aminotransferase; BCAA, branched-chain amino acids; CLND, chemi-  
4 luminescent nitrogen detection; FBDD, fragment based drug discovery; DIPEA, diisopropyl  
5 ethylamine; HATU, 1-[Bis(dimethylamino)methylene]-1*H*-1,2,3-triazolo[4,5-*b*]pyridinium 3-  
6 oxide hexafluorophosphate; HTS, high throughput screening; LE, ligand efficiency; LLE<sub>AT</sub>,  
7 lipophilic ligand efficiency defined by Astex; PK, pharmacokinetic; PLP pyridoxal phosphate;  
8 PMP, pyridoxamine phosphate; PPB, plasma protein binding; SAR, structure-activity  
9 relationship; STD-NMR, saturation-transfer difference nuclear magnetic resonance; T<sub>m</sub>, thermal  
10 shift.  
11  
12  
13  
14  
15  
16  
17  
18  
19  
20

## 21 REFERENCES

- 22  
23  
24  
25 1. Sweatt, A. J.; Wood, M.; Suryawan, A.; Wallin, R.; Willingham, M. C.; Hutson, S. M.  
26 Branched-chain Amino Acid Catabolism: Unique Segregation of Pathway Enzymes in Organ  
27 Systems and Peripheral Nerves. *Am. J. Physiol. -Endoc. M.* **2004**, *286*, E64-E76.  
28  
29  
30  
31  
32  
33 2. She, P.; Reid, T. M.; Bronson, S. K.; Vary, T. C.; Hajnal, A.; Lynch, C. J.; Hutson, S. M.  
34 Disruption of BCAT<sub>m</sub> in Mice Leads to Increased Energy Expenditure Associated with the  
35 Activation of a Futile Protein Turnover Cycle. *Cell Metab.* **2007**, *6*, 181-194.  
36  
37  
38  
39  
40  
41 3. She, P.; Zhou, Y.; Zhang, Z.; Griffin, K.; Gowda, K.; Lynch, C. J. Disruption of BCAA  
42 Metabolism in Mice Impairs Exercise Metabolism and Endurance. *J. Appl. Physiol.* **2010**, *108*,  
43 941-949.  
44  
45  
46  
47  
48  
49 4. Bertrand, S. M.; Ancellin, N.; Beaufils, B.; Bingham, R. P.; Borthwick, J. A.; Boullay, A.  
50 B.; Boursier, E.; Carter, P. S.; Chung, C. W.; Churcher, I.; Dodic, N.; Fouchet, M. H. ; Fournier,  
51 C.; Francis, P. L.; Gummer, L. A.; Herry, K.; Hobbs, A.; Hobbs, C. I.; Homes, P.; Jamieson, C.;  
52 Nicodeme, E.; Pickett, S. D.; Reid, I. H.; Simpson, G. L.; Sloan, L. A.; Smith, S. E.; Somers, D.  
53  
54  
55  
56  
57  
58  
59  
60

1  
2  
3 O.; Spitzfaden, C.; Suckling, C. J.; Valko, K.; Washio, Y.; Young, R. J. The Discovery of in  
4  
5 Vivo Active Mitochondrial Branched-Chain Aminotransferase (BCATm) Inhibitors by  
6  
7 Hybridizing Fragment and HTS Hits. *J. Med. Chem.* **2015**, *58*, 7140-7163.

8  
9  
10  
11 5. Deng, H.; Zhou, J.; Sundersingh, F. S.; Summerfield, J.; Somers, D.; Messer, J. A.; Satz, A.  
12  
13 L.; Ancellin, N.; Arico-Muendel, C. C.; Bedard, K. L.; Beljean, A.; Belyanskaya, S. L.;  
14  
15 Bingham, R.; Smith, S. E.; Boursier, E.; Carter, P.; Centrella, P. A.; Clark, M. A.; Chung, C. W.;  
16  
17 Davie, C. P.; Delorey, J. L.; Ding, Y.; Franklin, G. J.; Grady, L. C.; Herry, K.; Hobbs, C.;  
18  
19 Kollmann, C. S.; Morgan, B. A.; Kaushansky, L. J.; Zhou, Q. Discovery, SAR, and X-ray  
20  
21 Binding Mode Study of BCATm Inhibitors from a Novel DNA-Encoded Library. *ACS Med.*  
22  
23 *Chem. Lett.* **2015**, *6*, 919-924.

24  
25  
26  
27  
28  
29 6. Scanlon, M. Inhibitors of BCATm: A Tough Nut To Crack. *J. Med. Chem.* **2015**, *58*, 7138-  
30  
31 7139.

32  
33  
34  
35 7. Whittaker, M.; Law, R. J.; Ichihara, O.; Hesterkamp, T.; Hallett, D. Fragments: Past,  
36  
37 Present and Future. *Drug Discov. Today: Technologies* **2010**, *7* e163-e171.

38  
39  
40  
41 8. Schiebel, J.; Radeva, N.; Köster, H.; Metz, A.; Krotzky, T.; Kuhnert, M.; Diederich, W. E.;  
42  
43 Heine, A.; Neumann, L.; Atmanene, C.; Roecklin, D.; Vivat-Hannah, V.; Renaud, J. P.;  
44  
45 Meinecke, R.; Schlinck, N.; Sitte, A.; Popp, F.; Zeeb, M.; Klebe, G. One Question, Multiple  
46  
47 Answers: Biochemical and Biophysical Screening Methods Retrieve Deviating Fragment Hit  
48  
49 Lists. *ChemMedChem* **2015**, *10*, 1511-1521.

50  
51  
52  
53 9. Alex, A. A.; Flocco, M. M. Fragment-Based Drug Discovery: What has it Achieved so  
54  
55 Far? *Curr. Top. Med. Chem.* **2007**, *7*, 1544-1567.

- 1  
2  
3  
4  
5  
6  
7  
8  
9  
10  
11  
12  
13  
14  
15  
16  
17  
18  
19  
20  
21  
22  
23  
24  
25  
26  
27  
28  
29  
30  
31  
32  
33  
34  
35  
36  
37  
38  
39  
40  
41  
42  
43  
44  
45  
46  
47  
48  
49  
50  
51  
52  
53  
54  
55  
56  
57  
58  
59  
60
10. Chessari, G.; Woodhead, A. J. From Fragment to Clinical Candidate – a Historical Perspective. *Drug Discov. Today* **2009**, *14*, 668-675.
  11. Hajduk, P. J.; Greer, J. A Decade of Fragment-Based Drug Design: Strategic Advances and Lessons Learned. *Nat. Rev. Drug Discov.* **2007**, *6*, 211-219.
  12. Hutson, S. Structure and Function of Branched Chain Aminotransferases. *Progress in Nucleic Acid Research and Molecular Biology*, **2001**, *70*, 175-206. Academic Press, San Diego.
  13. Hann, M. M.; Leach, A. R.; Harper, G. Molecular Complexity and its Impact on the Probability of Finding Leads for Drug Discovery. *J. Chem. Inf. Comp. Sci.* **2001**, *41*, 856-864.
  14. Ludwig, C.; Guenther, U. L. Ligand Based NMR Methods for Drug Discovery. *Front Biosci.* **2009**, *14*, 4565-4574.
  15. Gozalbes, R.; Carbajo, R. J.; Pineda-Lucena, A. Contributions of Computational Chemistry and Biophysical Techniques to Fragment-Based Drug Discovery. *Curr. Med. Chem.* **2010**, *17*, 1769-1794.
  16. Hopkins, A. L.; Groom, C. R.; Alex, A. Ligand Efficiency: a Useful Metric for Lead Selection. *Drug Discov. Today* **2004**, *9*, 430-431.
  17. Mortenson, P.; Murray, C. Assessing the Lipophilicity of Fragments and Early Hits. *J. Comput. -Aided Mol. Des.* **2011**, *25*, 663-667.
  18. Fischer, M.; Hubbard, R. E. Fragment-Based Ligand Discovery. *Mol. Interv.* **2009**, *9*, 22-30.

- 1  
2  
3 19. Ishikawa, M.; Hashimoto, Y. Improvement in Aqueous Solubility in Small Molecule Drug  
4  
5 Discovery Programs by Disruption of Molecular Planarity and Symmetry. *J. Med. Chem.* **2011**,  
6  
7 54, 1539-1554.  
8  
9
- 10  
11 20. Murray, C. W.; Rees, D. C. The Rise of Fragment-Based Drug Discovery. *Nat. Chem.*  
12  
13 **2009**, *1*, 187-192.  
14  
15
- 16  
17 21. Azizian, J.; Mohammadi, A. A.; Karimi, A. R.; Mohammadizadeh, M. R. A Stereoselective  
18  
19 Three-Component Reaction:  $KAl(SO_4)_2 \cdot 12H_2O$ , an Efficient and Reusable Catalyst for the One-  
20  
21 Pot Synthesis of cis-Isoquinolonic Acids. *J. Org. Chem.* **2004**, *70*, 350-352.  
22  
23
- 24  
25 22. Willett, P.; Barnard, J. M.; Downs, G. M. Chemical Similarity Searching. *J. Chem. Inf.*  
26  
27 *Comp. Sci.* **1998**, *38*, 983-996.  
28  
29
- 30  
31 23. Tversky, A. Features of Similarity. *Psychol. Rev.* **1977**, 327-352.  
32  
33
- 34  
35 24. Harper, G.; Bravi, G. S.; Pickett, S. D.; Hussain, J.; Green, D. V. S. The Reduced Graph  
36  
37 Descriptor in Virtual Screening and Data-Driven Clustering of High-Throughput Screening Data.  
38  
39 *J. Chem. Inf. Comp. Sci.* **2004**, *44*, 2145-2156.  
40  
41
- 42  
43 25. Bailey, S. The CCP4 Suite: Programs for Protein Crystallography. *Acta Crystallogr.*,  
44  
45 *Sect.D: Biol.Crystallogr.* **1994**, 760-763.  
46  
47  
48  
49  
50  
51  
52  
53  
54  
55  
56  
57  
58  
59  
60

1  
2  
3  
4  
5  
6  
7  
8  
9  
10  
11  
12  
13  
14  
15  
16  
17  
18  
19  
20  
21  
22  
23  
24  
25  
26  
27  
28  
29  
30  
31  
32  
33  
34  
35  
36  
37  
38  
39  
40  
41  
42  
43  
44  
45  
46  
47  
48  
49  
50  
51  
52  
53  
54  
55  
56  
57  
58  
59  
60

Insert Table of Contents Graphic and Synopsis Here

